AD-766 050

EFFECT OF FREQUENCY AND TEMPERATURE ON ROCK DIELECTRIC PROPERTIES

Aida S. Khalafalla

Honeywell, Incorporated

Prepared for:

Bureau of Mines
Advanced Research Projects Agency

July 1973

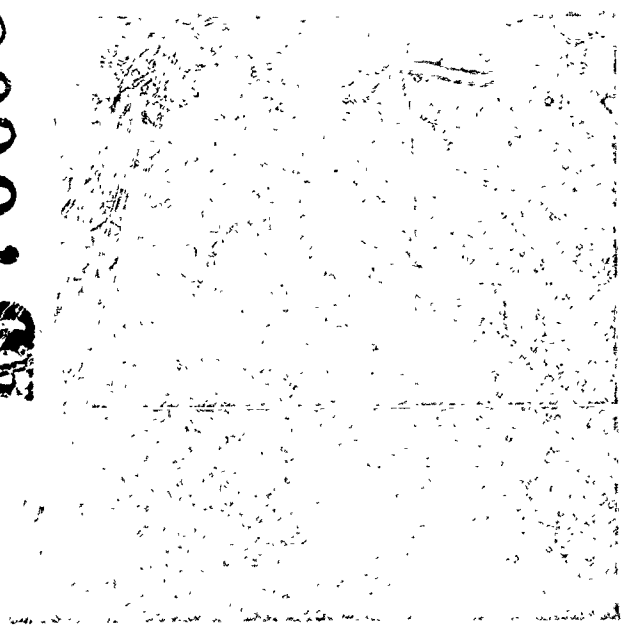

HONEYWELL

SYSTEMS & RESEARCH DIVISION

July 1973

Effect of Frequency and Temperature on Rock Dielectric Properties

Final Report

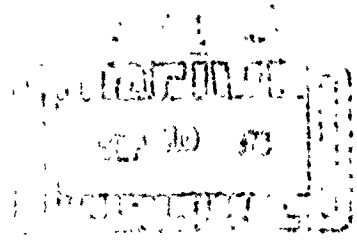

2816-3001

Unclassified
Security Classification

DOCUMENT CONTROL DATA - R & D

Security classification of title, body of abstract and indexing annotation must be entered when the overall report is classified

1 ORIGINATING ACTIVITY (Corporate author) Honeywell Inc. Systems and Research Center 2600 Ridgway Parkway; Minneapolis, Minn.	2a. REPORT SECURITY CLASSIFICATION Unclassified 2b. GROUP

3 REPORT TITLE

"Effect of Frequency and Temperature on Rock Dielectric Properties"
(Final Report)

4 DESCRIPTIVE NOTES (Type of report and inclusive dates)

Final Report 6/15/72 - 6/14/73

5 AUTHOR(S) (First name, middle initial, last name)

Aida S. Khalafalla

6 REPORT DATE	7a. TOTAL NO. OF PAGES	7b. NO OF REFS
15 July 1973	76	10

8a. CONTRACT OR GRANT NO. H0220054 b. PROJECT NO ARPA Order No. 1579, Amend. 3 c d	9a. ORIGINATOR'S REPORT NUMBER(S) 2816-3001 9b. OTHER REPORT NO(S) (Any other numbers that may be assigned this report)

10 DISTRIBUTION STATEMENT

Distribution of this document is unlimited.

11 SUPPLEMENTARY NOTES	12. SPONSORING MILITARY ACTIVITY
	Advanced Research Projects Agency Washington, D. C., 20301

13 ABSTRACT

The real and imaginary components of dielectric constant were determined for basalt, granite and quartzite in the frequency range 10MHz to 4 GHz. The variation of dielectric permittivity with temperature was determined from room temperature to 450°C. No dielectric dispersion or rock relaxation was observed in the frequency range investigated. Hence, the rock relative dielectric constant and relative loss showed mild variation with frequency with no discontinuity or sharp peaks as those previously observed in the low frequency range (up to 2 KHz). The temperature coefficient of the relative dielectric constant was related to the isobarric thermal expansion coefficient of the rock. The relative dielectric loss of basalt and granite followed an Arrhenius exponential increase with temperature suggesting the loss mechanism to be associated with activated particulate diffusion in the rock lattice. Activation energy for the conductance process depended on the temperature range and appeared to be independent of frequency. Quartzite showed an anomalous temperature variation of its conductivity.

DD FORM 1 NOV 68 1473 REPLACES DD FORM 1473, 1 JAN 64, WHICH IS OBSOLETE FOR ARMY USE.

Unclassified
Security Classification

14 KEY WORDS	LINK A		LINK B		LINK C	
	ROLE	WT	ROLE	WT	ROLE	WT
Dielectric						
Rock						
Conductivity						
Loss Tangent						
Frequency						
Permittivity						
Polarization						
Basalt						
Granite						
Quartzite						

ia

Final Report July 1973

EFFECT OF FREQUENCY AND TEMPERATURE ON ROCK DIELECTRIC PROPERTIES

Sponsored by

Advanced Research Projects Agency
ARPA Order No. 1579, Amendment 3
Program Code No. 2F10

Contract No. H0220054
Amount of Contract: $39,570
Effective Date of Contract: June 1972
Contract Expiration Date: June 1973

Contractor

Honeywell Inc.
Systems and Research Center
2600 Ridgway Parkway
Minneapolis, Minnesota

ACKNOWLEDGEMENT

This research was supported by the Advanced Research Projects Agency of the Department of Defense and was monitored by the U.S. Bureau of Mines under Contract No. H0220054.

Prepared by: Aida Khalafalla
A.S. Khalafalla / PhD
Sr. Principal Research Scientist
Tel. 612/331-4141, Ext. 4555

Approved by: Jaan Jurrison
Jaan Jurrison
Supervisor
Material Science Group
Tel. 612/331-4141, Ext. 5801

ACKNOWLEDGEMENT

The assistance of Principal Research Engineer Lyle Koehler and Research Assistant John Viner is gratefully acknowledged for their contribution to the electronic and engineering aspects of this research effort.

CONTENTS

ILLUSTRATIONS

TABLES

SECTION I
PROJECT OBJECTIVES AND SIGNIFICANT RESULTS

RESEARCH OBJECTIVES

The goal of this research was to develop reliable methods to measure the dielectric permittivity of rocks at high frequencies and at high temperatures. The real and imaginary parts of the dielectric constant were determined for three rock samples in the frequency range 10 MHz to 4 GHz. Measurement temperature was varied from room temperature to 450°C. The temperature coefficient of the dielectric constant was used to derive other rock thermophysical properties such as the coefficient of thermal expansion and the activation energy for ionic or vacancy diffusion in the rock. The data thus obtained and their scientific analysis are relevant to solving such practical problems as dielectric heating and rock fragmentation by electrothermal methods.

SIGNIFICANT RESULTS

Determination of the standing wave pattern in rock samples allowed measurement of their electrical parameters in the frequency range 0.2 to 2 GHz. The data from the slotted-line technique were checked with those determined by the conventional bridge-balancing techniques at the overlap frequency range; i.e., that range at which both methods are applicable.

Dielectric constants and dissipation factors were determined for three rock samples over the 10 MHz to 2 GHz frequency range. The real part, ϵ_r', of the relative complex permittivity decreases slightly with increasing frequency up to 20 MHz. From 0.2 to 2 GHz, ϵ_r' increases slowly with frequency. The

loss tangent, tan δ, decreases slowly with frequency in the entire frequency range. Both the relative dielectric constant and the loss factor increase with temperature rise.

Application of the Clausius-Mosotti relationship to the relative dielectric constant of rocks allows an estimation of their thermal coefficient of volume expansion at a series of temperatures. This method, which is reported here for the first time, may be used instead of the commonly used thermal dilatometric methods, especially for materials of low volume expansion coefficient.

Rock conductivities have been calculated from the relative dielectric loss. The variation with temperature of the rock conductivity appears to be fitted to an activated concept of ionic diffusion in the lattice. The activation energy, or the barrier height, for particle motion in the rock lattice has been determined for basalt and granite and found to depend on the temperature range but not on the frequency. An anomalous behavior was found in the variation with temperature of quartzite conductivity and was attributed to the evolution of water from the rock micropores.

SECTION II
INTRODUCTION

REVIEW OF DIELECTRIC MEASUREMENT TECHNIQUES

LUMPED-CIRCUIT MEASUREMENTS

At frequencies from dc to about 10^9 Hz, complex permittivity may be determined by lumped-circuit measurements. That is, the sample in its holder may be considered as part of a conventional R-L-C circuit. Typically, dielectric measurements of solid specimens at low frequencies are made on flat samples with parallel-plate electrodes.

Above 10^8 Hz the inductance of the electrodes can introduce serious measurement errors. Using resonant-cavity techniques, the measurement range can be extended to about 10^9 Hz. Beyond this frequency the sample dimensions are no longer negligible compared to the electrical wavelength, and distributed-circuit measurements must be used. A section of waveguide or transmission line which is partially filled with the specimen is typically used at UHF and microwave frequencies. The principles of transmission-line measurements follow directly from the relations involving ϵ^* and μ^* in the wave equations.

Coaxial transmission lines may be used for measurements at frequencies for which the conductor spacing is small compared to a wavelength; at higher frequencies it becomes necessary to use a hollow waveguide. Since the geometric relations for a coaxial capacitor are well defined, a coaxial-line sample holder may also be used for lumped-circuit measurements at low frequencies. The total measurement range of the coaxial-line technique extends from near dc to above 4 GHz.

For this study, the required measurement range is 10^7 Hz to 4×10^9 Hz. Measurements of complex permittivity were performed at temperatures from room temperature to 450°C. The coaxial-line technique is well suited for these measurements because it not only covers the entire frequency range but is also capable of withstanding the severe environment of the high-temperature measurements. Continuity of data is enhanced because the same rock specimens can be measured at all temperatures and frequencies.

COAXIAL-LINE MEASUREMENTS

At frequencies for which the section of line which comprises the sample holder is much less than one wavelength long, the holder may be considered as a coaxial capacitor, and its impedance Z at a frequency f is given by

$$Z = \frac{-j \ln\left(\frac{b}{a}\right)}{4\pi^2 f \epsilon_o \epsilon_r^* \ell} \qquad (2\text{-}1)$$

Where b and a are the radii of the outer and inner conductors, respectively, ℓ is the length of the holder, and ϵ_o is the permittivity of free space. (It is assumed here that the specimen completely fills the sample holder and that its permeability $\mu^* = \mu_o$.) Conventional bridge or resonance techniques may be used to determine Z.

When the length of the specimen is an appreciable fraction of a wavelength, it becomes necessary to treat the sample holder as a length of transmission line and to apply the line equations in order to extract ϵ_r^* from a measurement of the line input impedance. An open-circuit coaxial-line sample holder having a characteristic impedance Z_1, and propagation constant γ_1, when filled with a dielectric sample whose propagation constant is γ_2, will have an input impedance

$$Z_{in} = Z_1 \left(\frac{\gamma_1}{\gamma_2}\right) \coth \gamma_2 \ell \tag{2-2}$$

The propagation constant γ for a material whose complex permeability $\mu^* = \mu_o$ is given by

$$\gamma = j \frac{2\pi}{\lambda} (\epsilon_r^*)^{\frac{1}{2}} \tag{2-3}$$

If the sample length ℓ is sufficiently short, $\coth \gamma_2 \ell \simeq \frac{1}{\gamma_2 \ell}$. The error in this approximation is less than 3 percent when

$$\frac{2\pi\ell}{\lambda} (\epsilon_r^*)^{\frac{1}{2}} < 0.3 \tag{2-4}$$

Then the input impedance becomes

$$Z_{in} \simeq Z_1 \frac{\gamma_1}{\gamma_2^2 \ell} \tag{2-5}$$

and if the losses in the sample holder are negligible, $\gamma_1 = j(2\pi/\lambda)$ so that the expression further simplifies to

$$Z_{in} \simeq \frac{-j\lambda Z_1}{2\pi\epsilon_r^* \ell} \tag{2-6}$$

Then

$$\epsilon_r^* = \frac{-j\lambda Z_1}{2\pi\ell Z_{in}} \tag{2-7}$$

it can be shown that Equations (2-1) and (2-6) are identical, so that the condition $\frac{2\pi\ell}{\lambda}(\epsilon_r^*)^{1/2} < 0.3$ represents the short-wavelength limit for the validity of of the lumped-circuit coaxial capacitor measurement.

For a medium or low-loss dielectric sample ($\tan\delta_\epsilon < 0.1$) which has $\epsilon_r' = 10$, and $\ell = 10$ cm, the lumped-circuit approximation is valid at frequencies up to about 45 MHz.

R-X IMPEDANCE BRIDGE

To determine the input impedance of the coaxial line at frequencies below 2.5×10^8 Hz, a wide-range R-X bridge is used. The bridge used in our laboratory is a modified Schering bridge with a self-contained signal source and heterodyne detector. Figure 1 is a block diagram of the complete instrument, and Figure 2 is the equivalent circuit of the Schering bridge.

The bridge circuit operates over the frequency range from 0.5 to 250 MHz. It can measure equivalent parallel resistance, R_p, from 15 ohms to 10^5 ohms, and equivalent parallel capacitance, C_p, from -100 pf (inductive, $L_p = 1/\omega^2 C_p$) to + 20 pf. Because the capacitance of the coaxial holder plus sample generally exceeds 20 pf, a compensating inductance or reactive transmission-line stub is used to carry out the measurements.

SLOTTED-LINE MEASUREMENTS

A precision slotted line is used for measurements between 50 MHz and 4 GHz. In principle, the slotted line literally consists of a coaxial transmission line with a slot in its outer conductor through which a traveling rf-voltage or current probe may be inserted. A source of radio-frequency energy at the desired frequency drives the line, and the unknown impedance is connected to

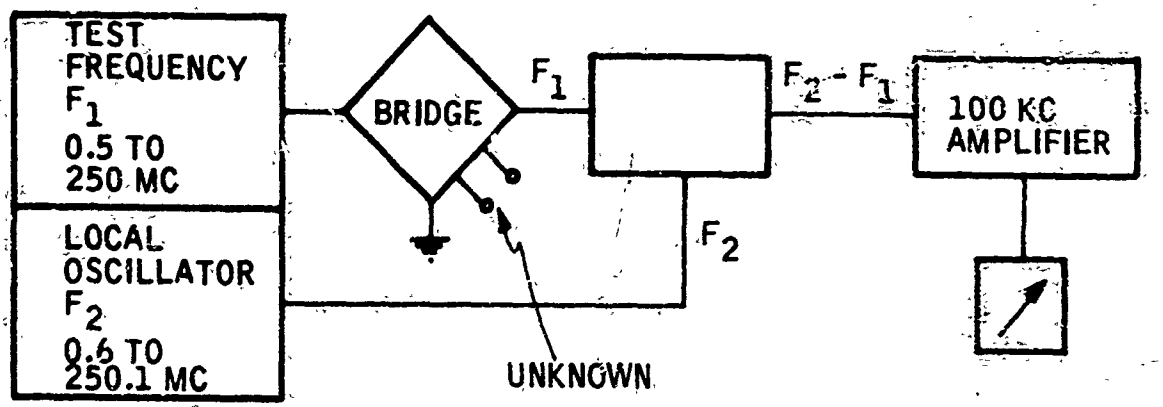

Figure 2-1. R-X Bridge Block Diagram

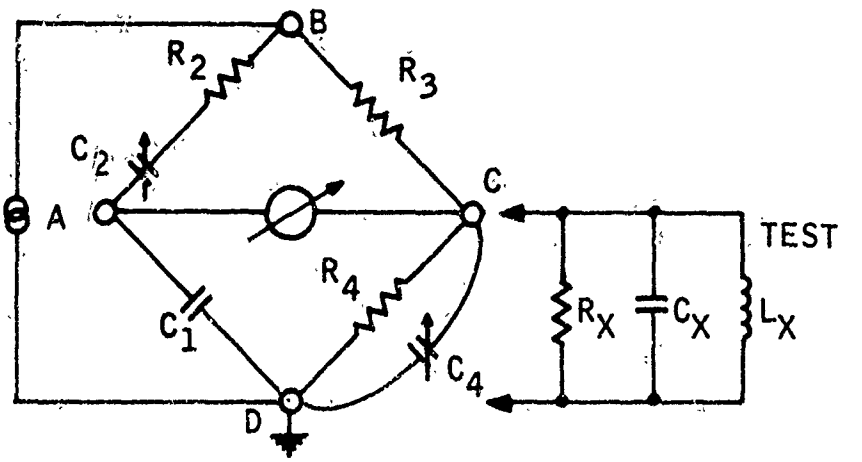

Figure 2-2. Schering Bridge Circuit

the opposite end. From the relative magnitudes and positions of the voltage or current maxima and minima, it is possible to calculate the complex impedance of the unknown.

A block diagram of the slotted-line measurement setup is shown in Figure 2-3. The signal source has a frequency range from 0.5 MHz to 4 GHz. Heterodyne detection of the voltage on the traveling probe is used rather than a square-law rectifier circuit. The heterodyne detector, consisting of the local oscillator, mixer, i-f amplifier, and voltmeter, actually corresponds to a sensitive receiver which can be tuned to the signal frequency. It provides high sensitivity and linear response as well as rejection of harmonics and other spurious signals.

Figure 2-4 is a photograph of the actual experimental configuration. From left to right the equipment functions are: power meter (above), signal oscillator (below), low-frequency signal oscillator plug-in unit, coaxial slotted line with mixer (front), local oscillator with power supply (rear), i-f amplifier-detector (rear), R-X impedance bridge with coaxial holder mounted, and oven.

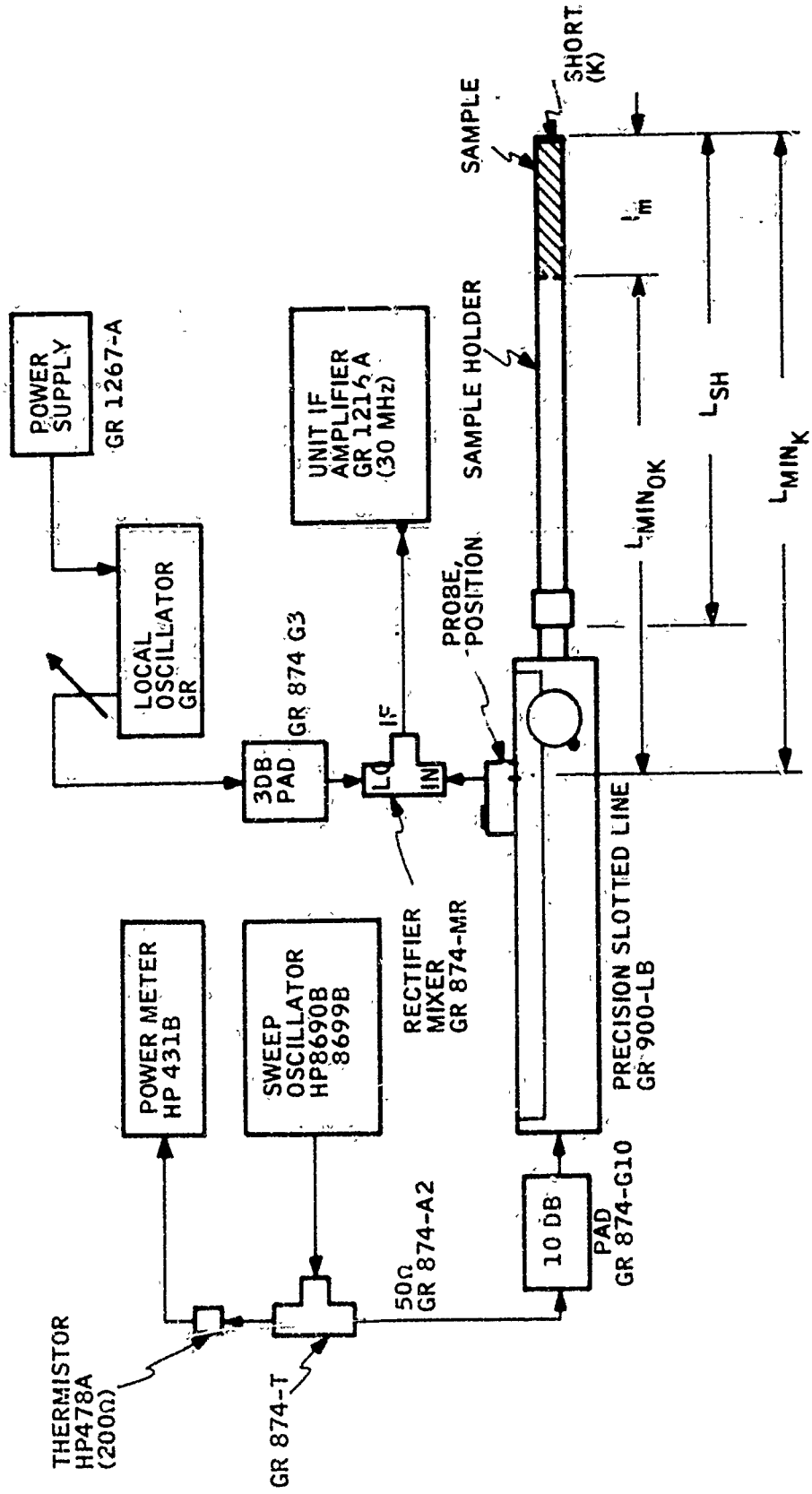

Figure 2-3. Heterodyne Slotted-Line System

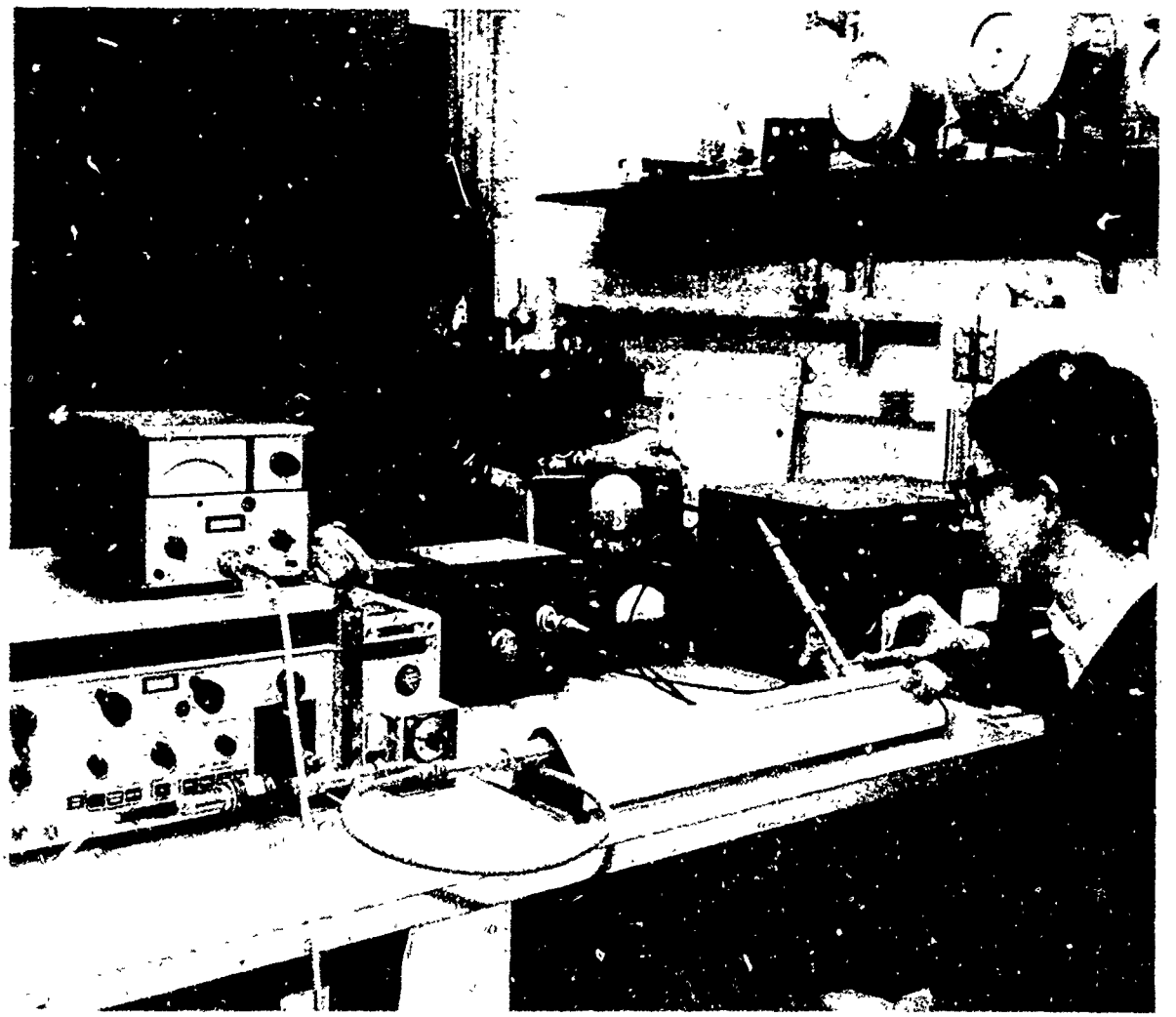

Figure 2-4. Experimental Configuration

SECTION III
EXPERIMENTAL WORK

SLOTTED-LINE MEASUREMENT PROCEDURE

Although the slotted-line technique involves measurement of the voltage standing-wave ratio (SWR = V max/V min) on the line, it is not necessary to measure the actual maximum and minimum voltages in all cases. When the SWR is high, it can be measured quite accurately by determining the width of a single null, defined as the distance between points at which the voltage is $\sqrt{2}$ times the minimum value. Thus, it is possible to use the slotted line even at frequencies for which the line is less than a half-wavelength long.

A number of procedures are commonly used for dielectric measurements with the slotted line (Refs. 1 and 2). Three specific cases are of special interest to us. They are (1) short-circuited sample holder, sample length a multiple of $\lambda/2$, (2) short-circuited sample holder, sample length an odd multiple of $\lambda/4$, and (3) open-circuited sample holder, sample length less than $\lambda/4$. Case 1 is preferred for measurements of ϵ_r' when the sample is at least a half-wavelength long. However, the error in determination of ϵ_r'' is greatest at half-wavelength intervals. Thus, the quarter-wave resonant condition of case 2 is used to obtain accurate measurements of dielectric loss. At lower frequencies, where the sample length does not permit "resonant" measurements, the best accuracy is offered by the open-circuited sample holder. Although the general solution of the transmission-line equations can be used to obtain measurements at any frequency, the resonant conditions are preferred because the computations are greatly simplified and the measurement errors are minimized.

An outline of the experimental procedure for measuring ϵ_r' and tan δ of a rock sample using resonance methods follows. Figure 3-1 shows the slotted line with both half-wave and quarter-wave sample resonance conditions.

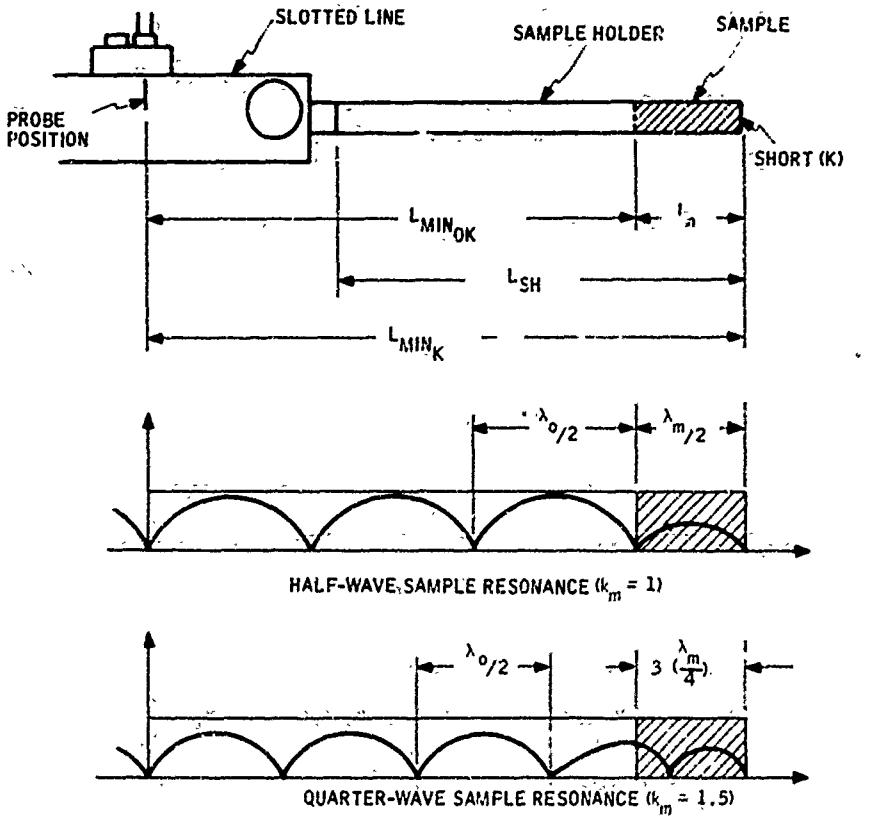

Figure 3-1. Dielectric Parameters from Resonance Methods

Consider first the half-wave resonance condition. With the sample of length ℓ_m inserted and shorted (K), the frequency (f) of the signal oscillator is adjusted until

$$k_m \left(\frac{\lambda_m}{2}\right) = \ell_m, \qquad k_m = 1, 2, \ldots \tag{3-1}$$

where λ_m is the sample wavelength. In addition,

$$n\left(\frac{\lambda_o}{2}\right) = L_{min}, \qquad n = 1, 2, \ldots \tag{3-2}$$

where λ_o is the empty-line wavelength and L_{min} is the distance from the rf probe to the sample. Under the above conditions and assuming $\tan \delta_e < 0.1$

$$\epsilon_r' = \left(\frac{\lambda_o}{\lambda_m}\right)^2 = \left(\frac{\lambda_o k_m}{2\ell_m}\right)^2 \qquad (3\text{-}3)$$

and ϵ_r' may be calculated from λ_o, k_m, and ℓ_m.

Next consider the quarter-wave resonance condition. With the sample of length ℓ_m inserted and shorted (K), the frequency (f) of the signal oscillator is adjusted until

$$2 k_m \left(\frac{\lambda_m}{4}\right) = k_m \left(\frac{\lambda_m}{2}\right) = \ell_m, \qquad k_m = 0.5,\ 1.5,\ 2.5,\ \ldots \qquad (3\text{-}4)$$

where λ_m is the sample wavelength. In addition

$$2n\left(\frac{\lambda_o}{4}\right) = n\left(\frac{\lambda_o}{2}\right) = L_{min}, \qquad n = 0.5,\ 1.5,\ 2.5,\ \ldots \qquad (3\text{-}5)$$

where λ_o is the empty-line wavelength and L_{min} is the distance from the rf probe to the sample. Under the above condition and assuming tan δ <0.1, then

$$\epsilon_r' = \left(\frac{\lambda_o}{\lambda_m}\right)^2 = \left(\frac{\lambda_o k_m}{2\ell_m}\right)^2 . \qquad (3\text{-}6)$$

The measurement of tan δ is made at quarter-wave resonance. The quarter-wave condition gives minimum error in tan δ because maximum field strength is applied to the sample. The inverse VSWR $\left(m = \frac{V_{min}}{V_{max}}\right)$ provides a measure of tan δ. To minimize rf probe loading, m can be found by measuring the width of minimum $\Delta\ell$. Then,

$$m = \frac{V_{min}}{V_{max}} = \frac{\left(\frac{\pi \Delta \ell}{\lambda_o}\right)}{\sqrt{1 + \sin^2\left(\frac{\pi \Delta \ell}{\lambda_o}\right)}} \qquad (3\text{-}7)$$

If $m < 0.1$, then to a good approximation

$$m \approx \frac{\pi \Delta \ell}{\lambda_o} \qquad (3\text{-}8)$$

With the sample in place, $\Delta \ell^*$ is measured at a voltage minimum under a quarter-wave sample resonance condition. $\Delta \ell^*$ gives m^* by using equation (3-8). The ratio m^* represents losses from three sources: (1) the sample of length ℓ_m; (2) the sample holder around the sample of length ℓ_m; and (3) the sample holder plus the slotted line of length $L_{min_{oK}}$.

Let $\Delta \ell_o$ and thus m_o represent the losses due to the length of line $L_{min_{oK}}$. Then

$$m_o \approx \frac{\pi \Delta \ell_o}{\lambda_o} \qquad (3\text{-}9)$$

The attenuation factor of the sample holder α_o gives a measure of the sample holder losses around the sample. Both $\Delta \ell_o$ and α_o may be experimentally determined by making width-of-minimum measurements on the empty and shorted sample holder.

Finally, knowing m^*, m_o, and α_o, then tan δ may be calculated from

$$\tan \delta = \frac{\lambda_o}{\pi} \left(\frac{m^* - m_o}{\ell_m \cdot \epsilon'_r} - \alpha_o \right) \qquad (3\text{-}10)$$

Again if m*, $m_o < 0.1$, then to a good approximation

$$\tan \delta = - \frac{\Delta \ell^* - \Delta \ell_o}{\ell_m \cdot \varepsilon_r'} = \frac{\lambda_o}{\pi} \alpha_o \qquad (3\text{-}11)$$

SAMPLE PREPARATION

One requirement for the coaxial-line technique is that the rock specimens must be prepared to fit precisely in a coaxial sample holder. The allowable tolerances are quite stringent; the specimen dimensions and tolerances for the nominal 14 mm coaxial-line sample holder are given below:

- Outside Diameter: 0.5625 $^{+0.000 \text{ in.}}_{-0.0028 \text{ in.}}$
- Hole Diameter: 0.24425 $^{+0.0012 \text{ in.}}_{-0.000 \text{ in.}}$
- Concentricity: ±0.005 in.

These tolerances are required for measurement errors below 10 percent in a low or medium loss sample with $\varepsilon_r' \leq 10$.

Samples with the required outer dimensions were supplied by the Bureau of Mines. To drill the center holes we used an ultrasonic drilling machine in which a diamond bit is simultaneously rotated and vibrated ultrasonically as it advances. This machine is capable of drilling precise holes up to 6 inches long in extremely hard materials. A photograph of a few drilled rock samples is shown in Figure 3-2.

Initial drilling efforts failed because of a mechanical misalignment in the machine which made it impossible to maintain concentricity between the inner and outer diameters. The machine had to be returned to the manufacturer. Although the problem was eventually corrected, the beginning of the measurement program was delayed by about two months.

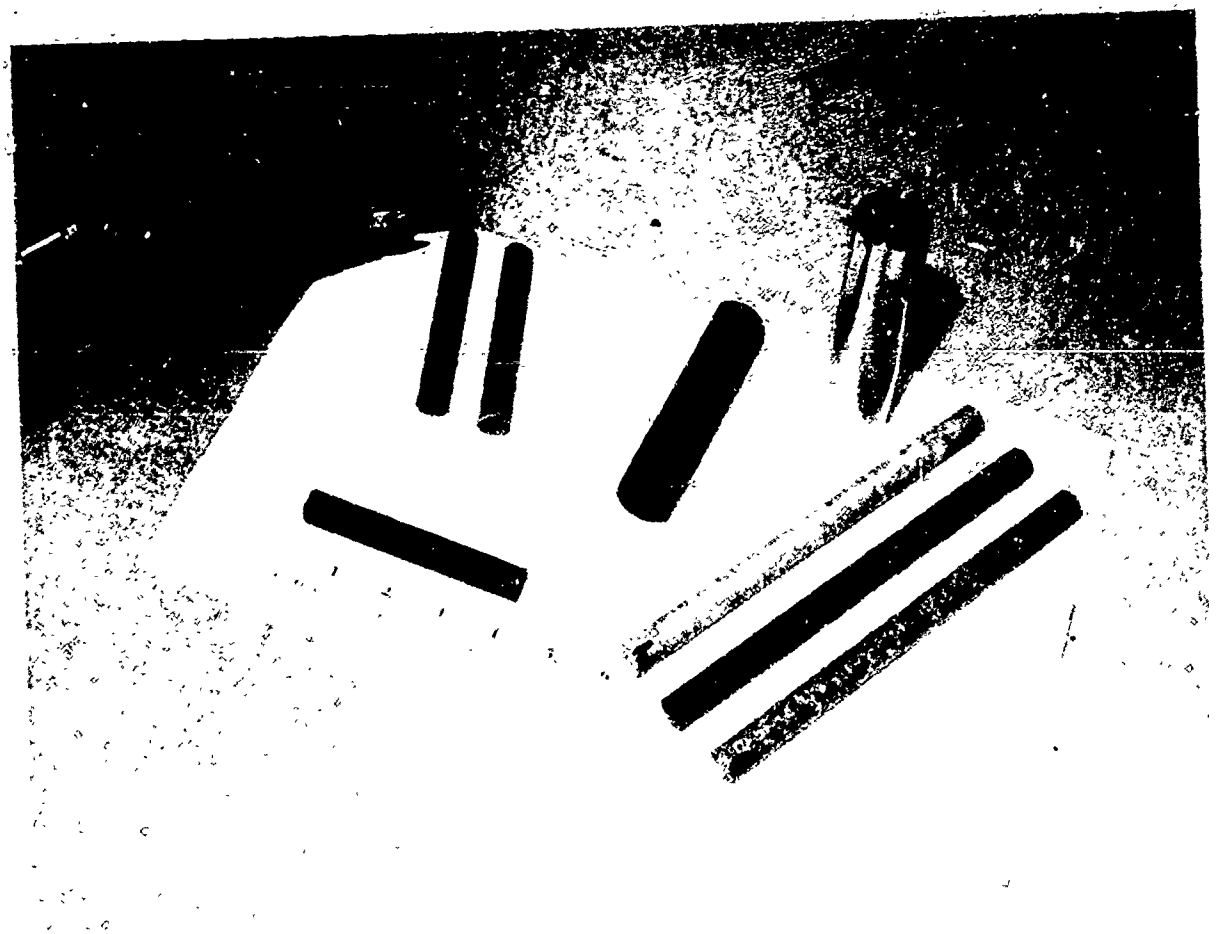

Figure 3-2. Samples of Drilled Rocks

Three samples of different geometry were measured for each rock type. Disk samples were measured with the parallel plate method; coaxial samples 25 mm in diameter were measured using the R-X bridge; and 14-mm coaxial samples were measured with the slotted-line technique. It was intended that several physically similar samples of each rock type would be measured to improve the statistical relevance of the data. Because of difficulties in sample preparation, coupled with the time consumed in obtaining each data point at a given frequency and temperature, it was impractical to repeat the measurement sequence for multiple samples.

HIGH TEMPERATURE MEASUREMENTS

Measurements at other than room temperature were conducted with the coaxial sample holder inside a controlled temperature chamber. This chamber accommodated a 30 cm sample length. Through a combination of electric heating and inert gas flow, the temperature was maintained at any predetermined value up to 450°C. A sketch of the oven, thermocouple and sample holder system is shown in Figure 3-3.

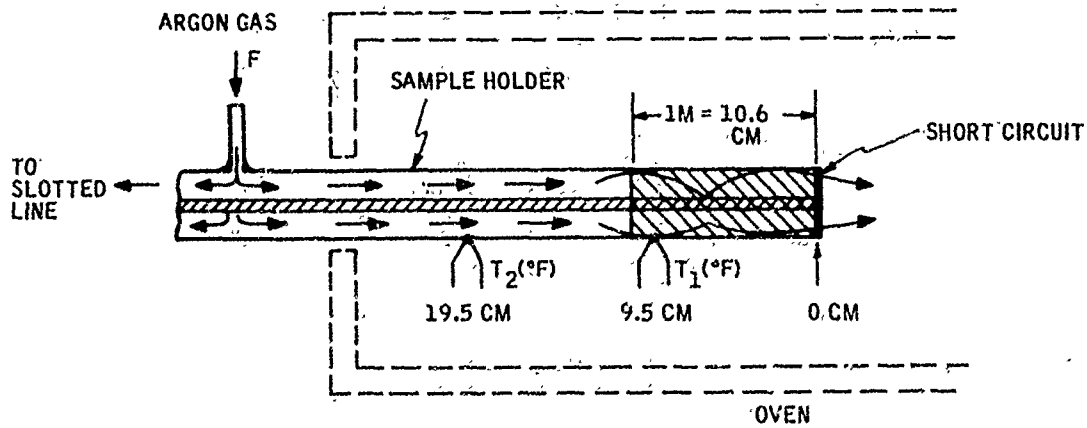

Figure 3-3. Rock Sample Heater for High Temperature Dielectric Data

Because of the coaxial sample holder's simple mechanical construction, the problems associated with the severe temperature environment are minimized. However, to protect the surfaces of the holder against corrosion at elevated temperature, an argon protective atmosphere was necessary. The coaxial transmission line between the measurement equipment (bridge or slotted line) was maintained at a slight positive pressure, using high-purity argon gas. Some gas will escape through the sample holder, maintaining a continuous flush of inert gas to sweep out reactive gases which may be driven out of the rock samples. In addition, by using two thermocouples in physical contact with the outer conductor of the sample holder, it was possible to measure and control the temperature of the rock sample at the desired setting.

SECTION IV
ROCK DIELECTRIC PROPERTIES IN THE MEGA- AND GIGA-HERTZ FREQUENCY RANGE

A Boonton type 250A RX meter was used to determine ϵ_r' and tan δ at room temperatures and at frequencies between 10 and 100 MHz. The rocks were cylindrical in shape with a diameter of 1.0 in. The granite rock was 0.250 in. long, while the basalt and quartzite samples were each 0.125 in. long.

Experimental data for basalt are given in Table 4-1. The variation of each of ϵ_r' and tan δ with frequency is shown in Figures 4-1 and 4-2. The results show that ϵ_r' is relatively constant, while tan δ decreases slightly from 10 to 70 MHz when both parameters begin to increase with increasing frequency.

The bridge data for the granite sample are shown in Table 4-2. Figures 4-3 and 4-4 illustrate the variation of granite dielectric parameters with frequency. Here again, ϵ_r' remains essentially constant at a value of slightly more than one-half of that of basalt up to a frequency of about 70 MHz. Above that frequency, ϵ_r' appears to rise appreciably with frequency. The loss tangent, on the other hand (Figure 4-4), was about one-third of that of basalt and decreased slowly with frequency.

The experimental data for the quartzite rock are given in Table 4-3. Variation of each of ϵ_r' and tan δ with frequency for quartzite is shown in Figures 4-5 and 4-6. Here ϵ_r' is about one-third that of basalt and appears to increase steadily with frequency, while tan δ is about one order of magnitude less than that of basalt and appears to increase with frequency above 70 MHz.

Table 4-1. Dielectric Parameters of Basalt, Bridge: Parallel-Plate Method

Basalt: Dimensions - t = 1.25 in., (t -- Rock-Sample Thickness); d_{SIL} = 0.875 in. (d_{SIL} -- Silver Electrode Diameter)
d_{ROCK} = 1.000 in. (d_{ROCK} -- Rock-Sample Diameter)

f(MHz)	C_p'(pf)	R_p'(KΩ)	C_{PH}(pf)	R_{PH}(KΩ)	C_p(pf) = $C_p' - C_{PH}$	R_p(KΩ)	X_p(KΩ)	R_s(Ω)	$-X_s$(KΩ)	*ϵ_r'	ϵ_r''	tan δ
10	15.70	15.6	1.59	>100M	14.11	15.6	1.02	65.5	1.02	13.05	0.847	6.49×10^{-2}
20	15.40	9.4	1.54	~10M	13.86	9.4	0.574	34.8	0.572	12.82	0.782	6.10×10^{-2}
40	15.52	5.0	1.56	>1M	13.96	5.0	0.285	16.1	0.284	12.91	0.735	5.69×10^{-2}
70	16.57	2.54	1.57	~1M	15.00	2.54	0.151	8.99	0.150	13.87	0.826	5.96×10^{-2}
100	18.87	1.34	1.56	500	17.31	1.34	0.0918	6.27	0.0914	16.01	1.097	6.85×10^{-2}
140	22.77	0.484	1.57	657	21.20	0.484	0.0536	5.86	0.0530	19.61	2.167	11.07×10^{-2}

*Assumes $d = d_{SIL}$

New Holder-Capacitance Correction and Average $d = \bar{d} = (d_{SIL} + d_{ROCK})/2$ = 0.938 in.

10		0.81	∞	14.89	15.6	1.07	73.1	1.07	11.97	0.821	6.86×10^{-2}
20		0.82	>1M	14.58	9.4	0.542	31.2	0.540	11.73	0.677	5.77×10^{-2}
40		0.83	>1M	14.69	5.0	0.271	14.6	0.270	11.82	0.641	5.42×10^{-2}
70		0.81	>1M	15.76	2.54	0.144	8.13	0.143	12.68	0.719	5.67×10^{-2}
100		0.82	>1M	18.05	1.34	0.0881	5.76	0.0878	14.53	0.956	6.57×10^{-2}
140		0.82	~500K	21.95	0.484	0.0517	5.49	0.511	17.57	1.89	10.7×10^{-2}

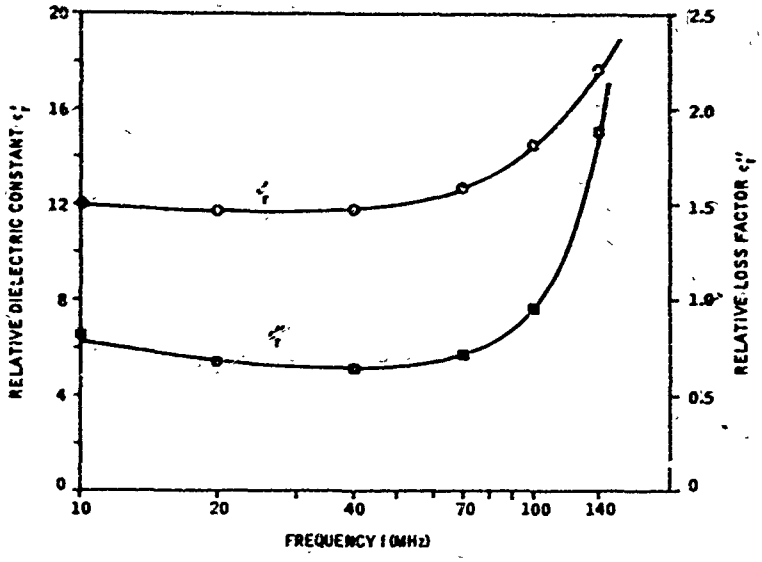

Figure 4-1. Relative Dielectric Constants of Basalt. Measurement with the R-X Meter using the Parallel-Plate Method

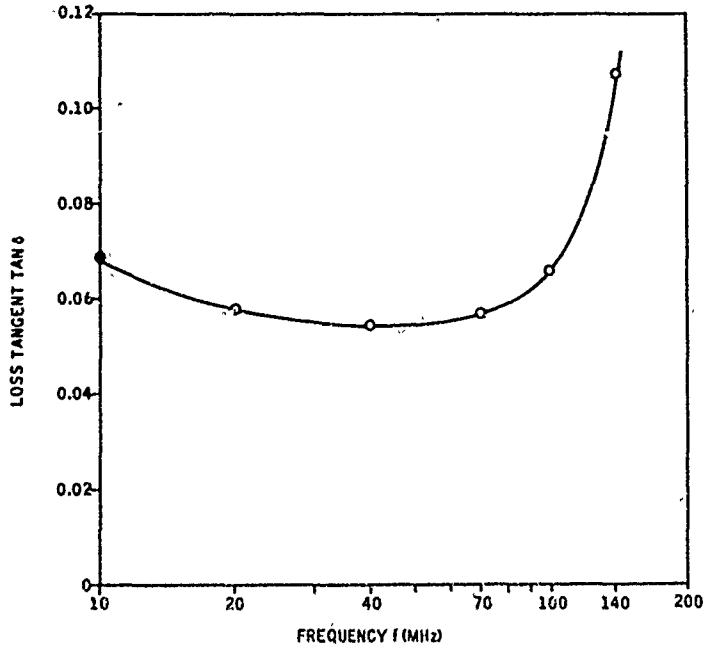

Figure 4-2. Loss Tangent of Basalt. Measurement with R-X Meter using the Parallel-Plate Method

Table 4-2. Dielectric Diameters of Granite. Bridge: Parallel-Plate Method

Granite: Dimensions - ℓ = 0.250 in. (ℓ -- Rock-Sample Thickness); d_{SIL} = 0.875 in. (d_{SIL} -- Silver Electrode Diameter)
d_{ROCK} = 1.000 in. (d_{ROCK} -- Rock-Sample Diameter)

f(MHz)	C_p'	R_p'(KΩ)	C_{PH}(pf)	R_{PH}(KΩ)	C_p(pf) = $C_p' - C_{PH}$	R_p(KΩ)	X_p(KΩ)	R_s(Ω)	$-X_s$(KΩ)	*ϵ_r'	ϵ_r''	tan δ
10	6.14	~200	1.80	>>100	4.26	200	3.74	700	3.74	7.88	1.47×10^{-1}	1.87×10^{-2}
20	6.14	80	1.88	>>100	4.26	80	1.87	434	1.87	7.88	1.84×10^{-1}	2.33×10^{-2}
40	6.18	46	1.83	>>100	4.30	46	0.924	119	0.824	7.95	1.28×10^{-1}	1.61×10^{-2}
70	6.33	27	1.88	>>100	4.45	27	0.511	96.5	0.511	8.23	1.55×10^{-1}	1.89×10^{-2}
100	6.67	18.7	1.88	>>100	4.79	18.7	0.332	59.3	0.332	8.86	1.58×10^{-1}	1.78×10^{-2}
140	7.42	11.8	1.92	~ 240	5.50	11.8	0.206	36.2	0.206	10.17	1.78×10^{-1}	1.75×10^{-2}

*Assumes d = d_{SIL}

New Holder-Capacitance Correction and Average d = $\bar{d}$ = $(d_{SIL} + d_{ROCK})/2$ = 0.938 in.

10		1.22	>1M	4.92	200	3.23	518	3.23	7.92	1.28×10^{-1}	1.61×10^{-2}
20		1.22	>1M	4.92	80	1.62	326	1.62	7.92	1.60×10^{-1}	2.02×10^{-2}
40		1.23	>1M	4.95	46	0.803	141	0.803	7.97	1.39×10^{-1}	1.75×10^{-2}
70		1.20	>1M	5.13	27	0.442	72.7	0.442	8.26	1.35×10^{-1}	1.64×10^{-2}
100		1.23	~1M	5.44	18.7	0.282	45.5	0.282	8.76	1.37×10^{-1}	1.56×10^{-2}
140		1.23	~0.9M	6.19	11.8	0.183	28.4	0.183	9.97	1.54×10^{-1}	1.55×10^{-2}

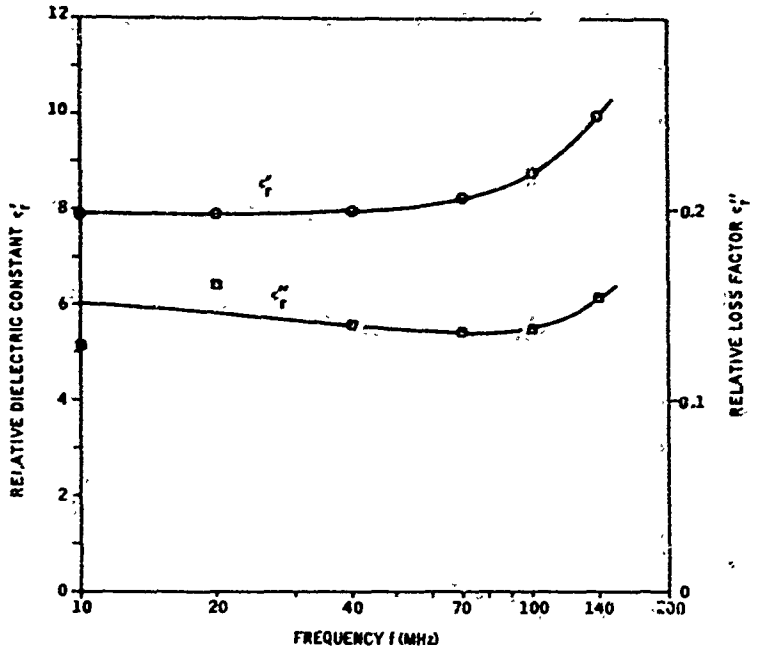

Figure 4-3. Dielectric Parameters of Granite Measured with the R-X Meter using the Parallel-Plate Method

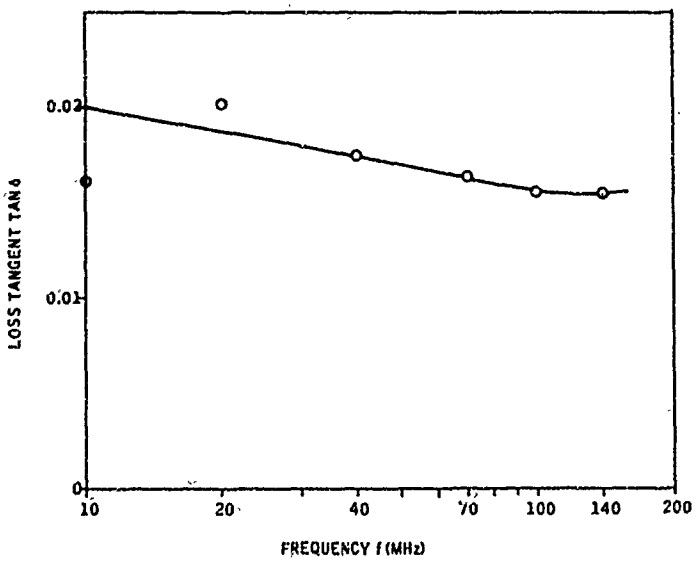

Figure 4-4. Loss Tangent of Granite Measured with the R-X Meter using the Parallel-Plate Method

Table 4-3. Dielectric Parameters of Quartzite. Bridge: Parallel-Plate Method

Quartzite Dimensions - t = 0.125 in. (t -- Rock-Sample Thickness); d_{SIL} = 0.875 in. (d_{SIL} -- Silver Electrode Diameter)
d_{ROCK} = 1.000 in. (d_{ROCK} -- Rock-Sample Diameter)

f(MHz)	C_p'(pf)	R_p'(KΩ)	C_{PH}(pf)	R_{PH}(Ω)	C_p(pf) = $C_p' - C_{PH}$	R_p(KΩ)	X_p(KΩ)	R_s(Ω)	$-X_p$(KΩ)	*ϵ_p'	ϵ_p''	tan δ
10	7.54	>1M	1.97	>10M	5.57	~1000	2.86	8.13	2.86	5.15	1.47×10^{-2}	2.85×10^{-3}
20	7.51	>500	1.93	>10M	5.58	~500	1.42	4.06	1.42	5.16	1.47×10^{-2}	2.85×10^{-3}
40	7.62	90	1.96	>1M	5.66	90	0.703	5.48	0.703	5.23	4.08×10^{-2}	7.80×10^{-3}
70	7.89	49	1.94	>1M	5.95	49	0.382	2.98	0.382	5.50	4.28×10^{-2}	7.79×10^{-3}
100	8.48	29.3	1.97	>1M	6.51	29.3	0.244	2.04	0.244	6.02	5.02×10^{-2}	8.34×10^{-3}
140	9.81	15.2	2.00	~75K	7.81	15.2	0.146	1.39	0.146	7.22	6.90×10^{-2}	9.57×10^{-3}

*Assumes $d = d_{SIL}$.

New Holder-Capacitance Correction and Average $d = \bar{d} = (d_{SIL} + d_{ROCK})/2$ = 0.938 in.

10		1.01	>10M	6.53	~1000	2.44	5.96	2.44	5.26	1.28×10^{-2}	2.44×10^{-3}
20		1.01	>10M	6.50	~500	1.22	2.98	1.22	5.23	1.28×10^{-2}	2.44×10^{-3}
40		1.00	>1M	6.62	90	0.600	4.01	0.600	5.33	3.56×10^{-2}	6.67×10^{-3}
70		1.02	>1M	6.87	49	0.331	2.32	0.331	5.53	3.74×10^{-2}	6.67×10^{-3}
100		1.02	>1M	7.46	29.3	0.213	1.55	0.213	6.00	4.36×10^{-2}	7.27×10^{-3}
140		1.02	~1M	8.79	15.2	0.129	1.09	0.129	7.07	6.00×10^{-2}	8.48×10^{-3}

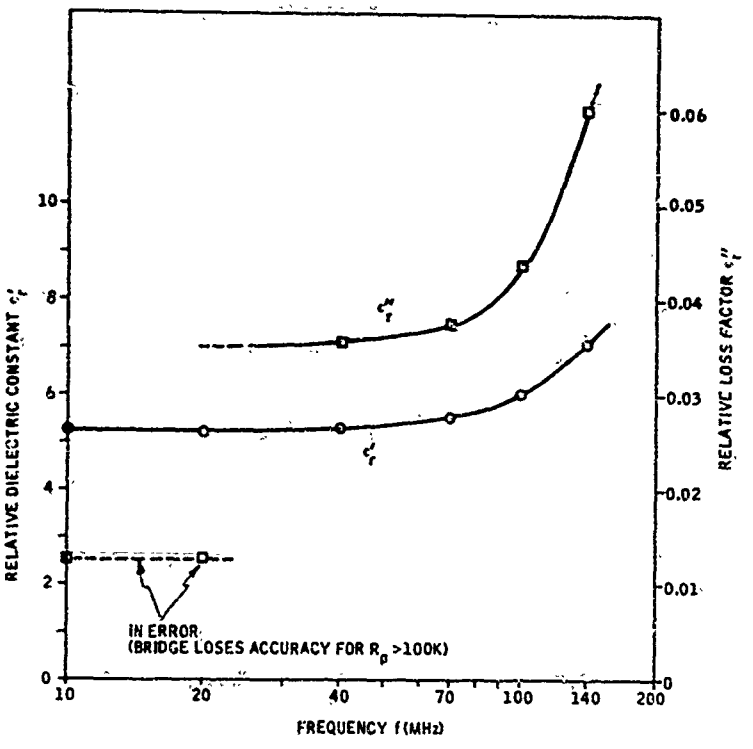

Figure 4-5. Dielectric Parameters of Quartzite Measured with the R-X Meter using the Parallel-Plate Method

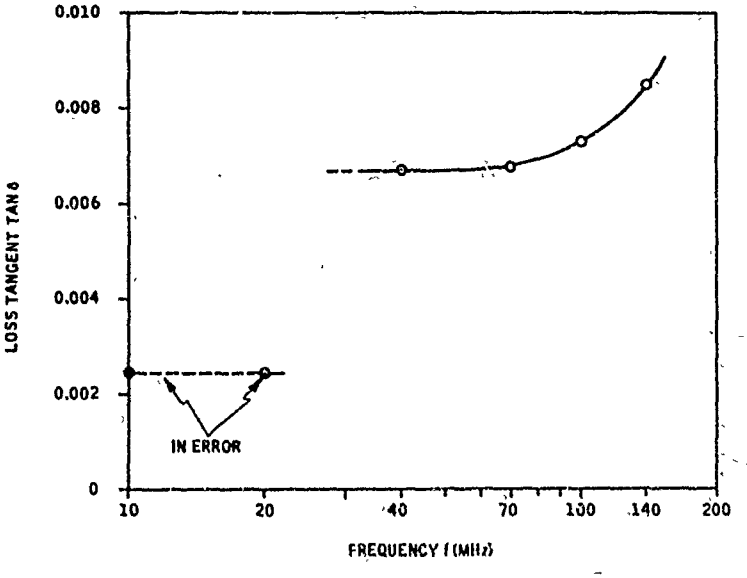

Figure 4-6. Loss Tangent of Quartzite Measured with the R-X Meter using the Parallel-Plate Method

BRIDGE MEASUREMENTS WITH COAXIAL SAMPLE HOLDER

Experimental data with the coaxial sample holder are given in Table 4 for the three rock samples. The frequencies used here did not exceed 50 MHz. The data obtained are not in essential agreement with those recorded with the cylindrical sample holder in the previous experiments. Figure 4-7 shows the variation of ϵ_r', ϵ_r'', and tan δ with frequency for basalt. Figures 4-8 and 4-9 illustrate the variation of these three parameters for granite and quartzite, respectively. As expected, the three dielectric parameters decrease slowly with increasing frequency.

SLOTTED-LINE MEASUREMENTS

Room temperature measurements were performed on a basaltic cylindrical sample of length 10.16 cm, with an outside diameter of 14 mm and an inside diameter of 6 mm. The data obtained are given in Table 4-5. The variation of the real part, ϵ_r', of the relative complex permittivity with frequency is shown in curve C of Figure 4-10. Curves A and B in the same figure show the measurements obtained with the bridge with parallel-plate sample holder and the bridge with coaxial sample holder, respectively. As is evident, the three techniques do not give identical results when measurements are made in the same frequency range; neither does the data follow the same trend at nearby frequency ranges.

Figure 4-11 shows the variation of the loss tangent of basalt with frequency. Curves A, B, and C depict the data obtained with the bridge (parallel-plate), the bridge with coaxial sample holder, and the slotted-line, respectively. Here the bridge data show a dissipation factor that decreases with frequency, while the slotted-line indicates an increasing loss factor with frequency. Here again, obvious discrepancies between the three methods are rather alarming.

Table 4-4. Bridge-Determined Rock Dielectric Data with Coaxial Sample Holder

f (MHz)	Cp(pf)	Rp(KΩ)	Xp(Ω)	ϵ_r'	ϵ_r''	tan δ
1. Basalt - ℓ = 11 cm						
9	82.35	1.73	191	13.8	1.71	0.124
18	78.88	1.02	99.9	13.4	1.31	0.110
50	78.32	0.407	40.3	13.1	1.31	0.0998
2. Granite - ℓ = 12.4 cm						
10	45.78	5.58	347	6.79	4.22×10^{-1}	6.22×10^{-2}
20	44.32	3.58	179	6.58	3.29×10^{-1}	5.00×10^{-2}
50	43.52	1.74	73.1	6.46	2.71×10^{-1}	4.20×10^{-2}
3. Quartzite - ℓ = 10.4 cm						
10	26.66	66.7	597	4.73	4.24×10^{-2}	8.95×10^{-3}
20	26.29	48.1	302	4.65	2.92×10^{-2}	6.28×10^{-3}
50	25.48	20.6	125	4.51	2.74×10^{-2}	6.07×10^{-3}

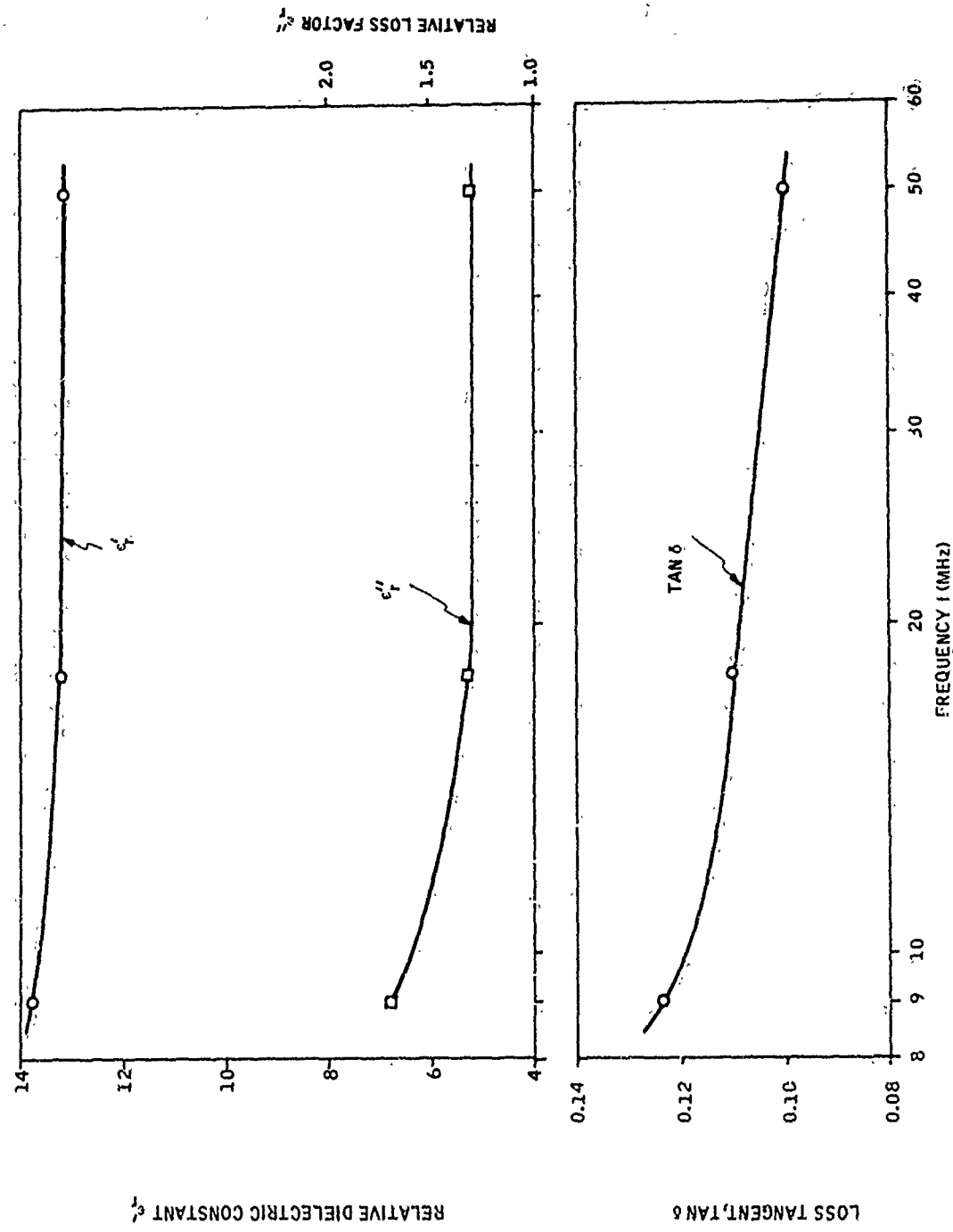

Figure 4-7. Dielectric Parameters of Basalt, Bridge Method with Coaxial Sample Holder

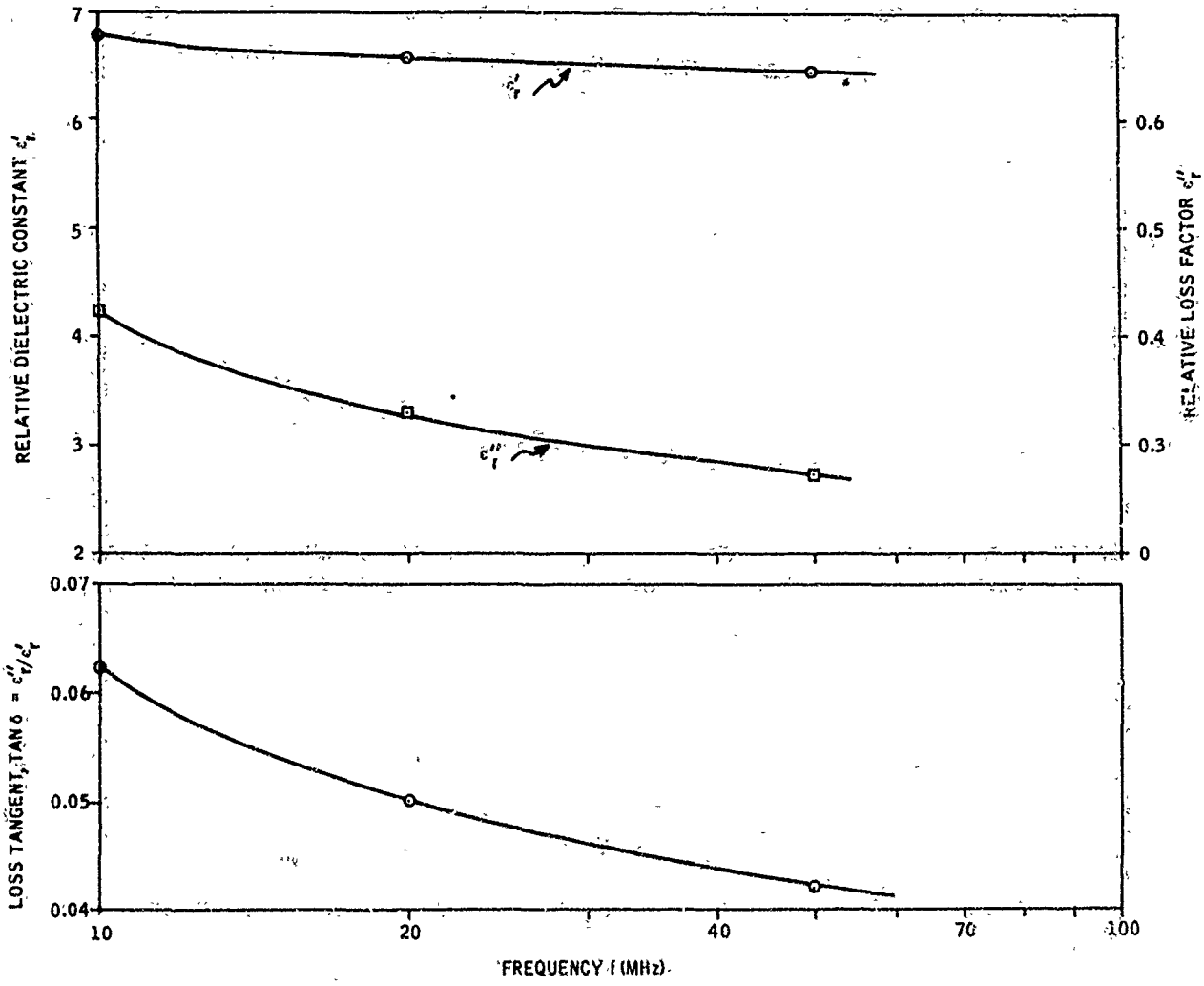

Figure 4-8. Dielectric Parameters of Granite. Bridge Method with Coaxial Sample Holder

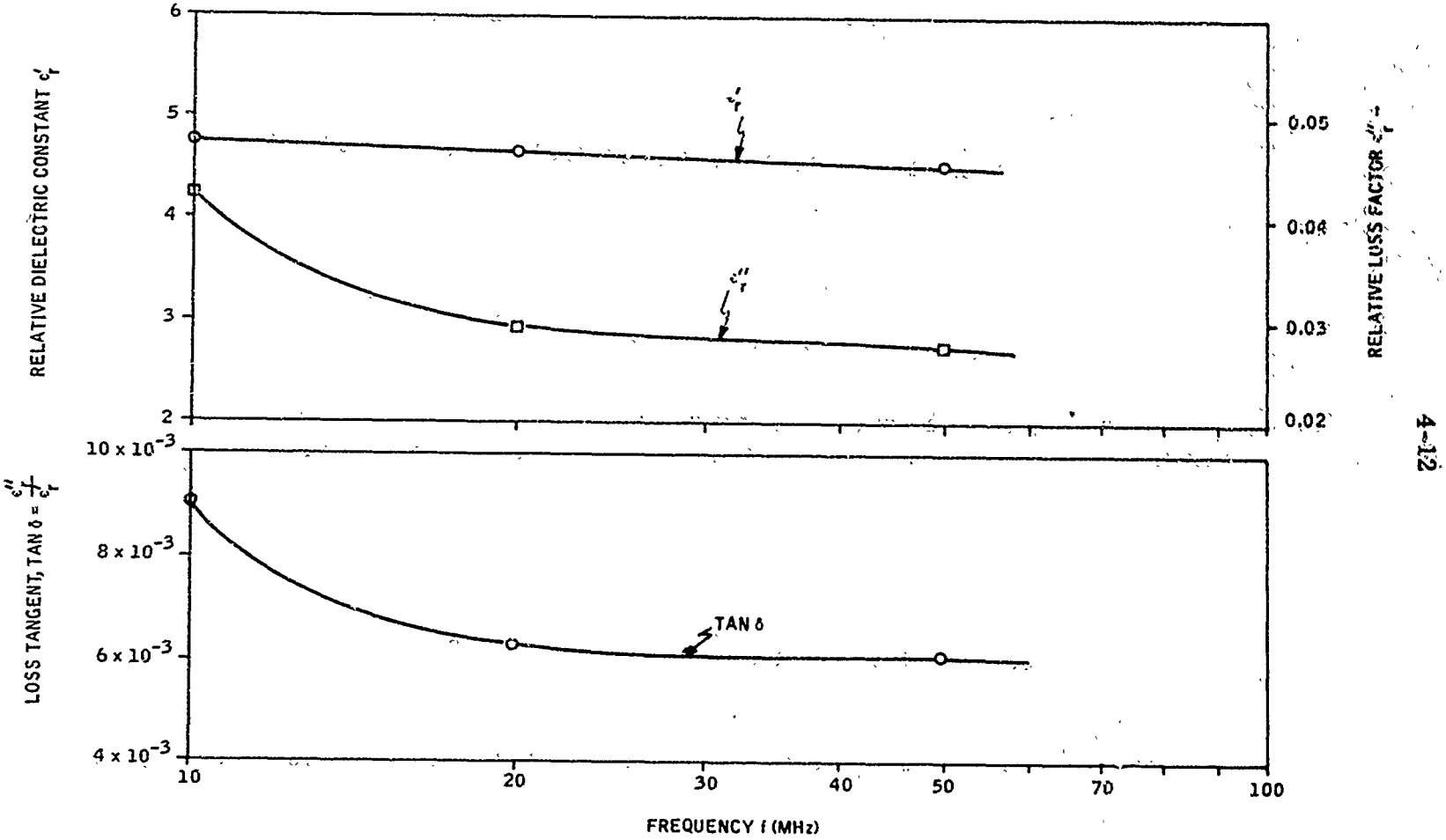

Figure 4-9. Dielectric Parameters of Quartzite, Bridge Method with Coaxial Sample Holder

Table 4-5. Dielectric Parameters of Basalt. Slotted-Line Method

Basalt: l_m = 10.16 cm; d_{out} = 14 mm, d_{in} = 6 mm; GR 874 Sample Holder; T = T_{ROOM} = 22°C.

Assumed l_{SH} (Sample Holder Length) = 43.65 cm for each data point.

l_{MIN} (cm)	f_{RES} (GHz)	$\lambda_{o_{RES}}$ (cm)	$\lambda_o/2$ (cm)	k_m	$\sqrt{\left(\frac{\lambda_o}{2}\right)^2 - \left(\frac{k_m}{\pi}\right)^2}$ ε_r'	Δl^* (cm)	$m^* = \frac{\sin\frac{\pi\Delta l^*}{\lambda_o}}{\sqrt{1+\sin^2\frac{\pi\Delta l^c}{\lambda_o}}}$	$\Delta l_c^* (\text{cm}) = \frac{\lambda_o}{\pi} m^*$	Δl_o (cm)	$\Delta l_c^* - \Delta l_o = \Delta l$(cm)	σ_o(mhos/cm) $\times 10^{-4}$	$\frac{\Delta l}{\varepsilon_r' m} = \frac{k_o}{\pi}\sigma_D + \tan\delta_\varepsilon$	ε_r''
16.58	0.238	126.1	63.1	0.5	9.63	5.08 (34.19 − 29.11)	0.1256	5.04	−0.22	4.81	0.83	0.0492 − 0.0033 = 0.0459	0.443
28.36	0.485	61.8	30.9	1.0	9.26								
18.86	0.715	41.94	20.97	1.5	9.61	5.65 (21.65 − 16.00)	0.380	5.08	0.0692	5.01	1.25	0.0814 − 0.0017 = 0.0492	0.477
13.68	0.953	31.5	15.8	2.0	9.68								
10.61	1.192	25.14	12.57	2.5	9.57	9.28 2(15.25 − 10.18)	0.676	5.41	0.0483	5.36	1.56	0.0552 − 0.0012 = 0.0540	0.517
19.11	1.427	21.05	10.52	3.0	9.64								
23.8	1.695	17.8	8.9	3.5	9.40		m = 0.96	5.44	0.0475	5.39	1.78	0.0565 − 0.0010 = 0.555	0.532
13.65	1.90	15.78	7.89	4.0	9.64								

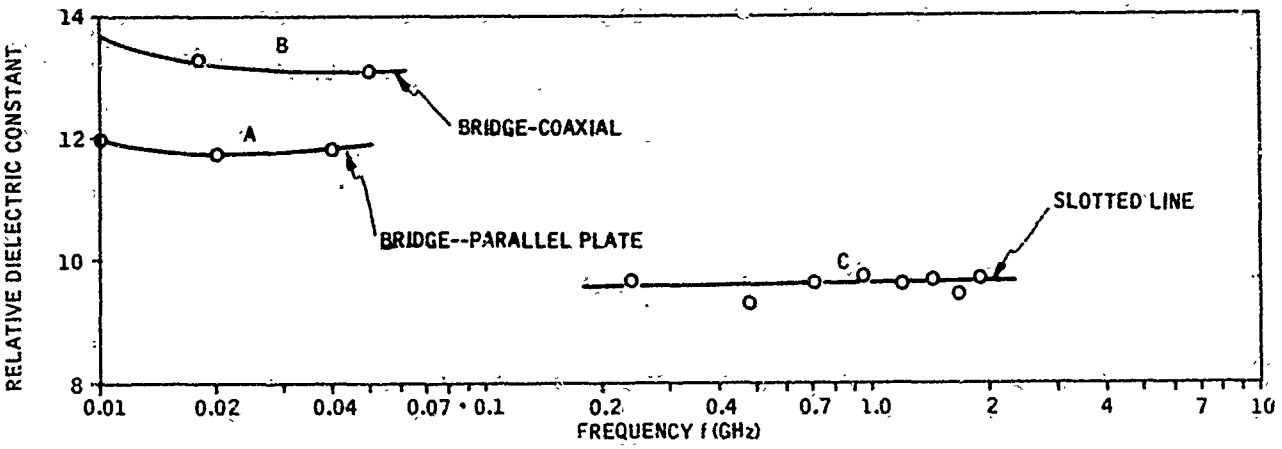

Figure 4-10. Relative Dielectric Constant of Basalt from 10 MHz to 2 GHz.

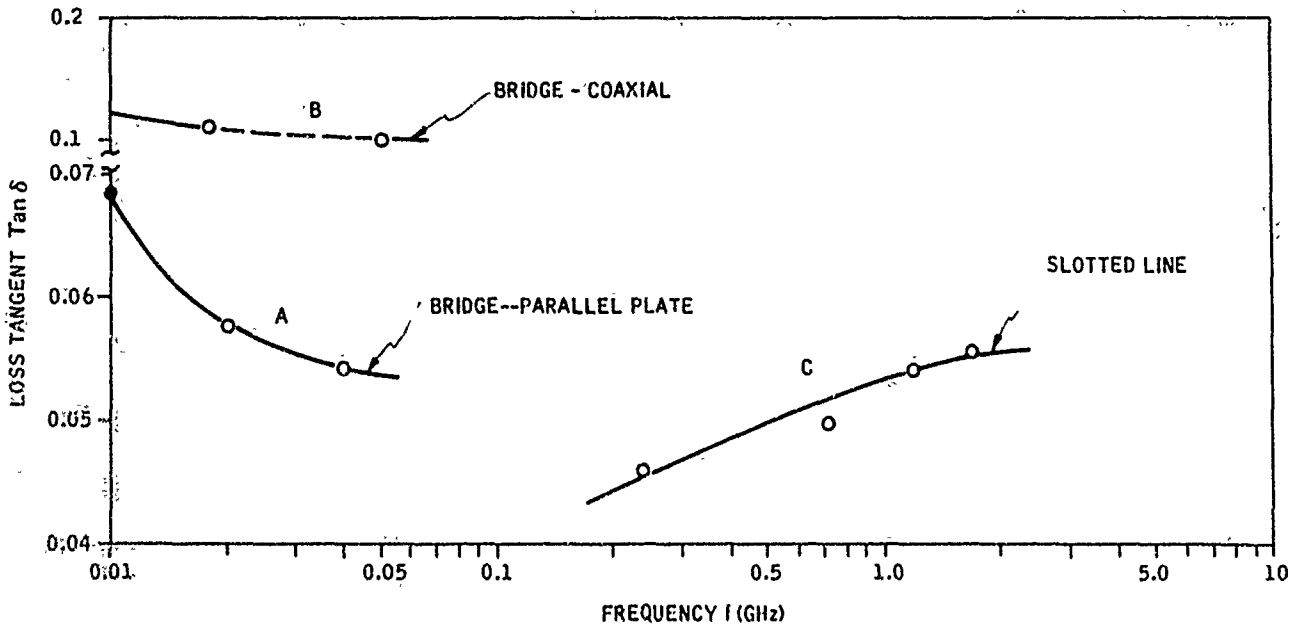

Figure 4-11. Loss Tangent of Basalt from 10 MHz to 2 GHz

Coaxial-line data of a granite sample with the same dimensions as the previous basaltic sample are given in Table 4-6. The relative dielectric constant, ϵ_r', increases slowly with frequency in the range 0.2 to 2 MHz as shown in curve C of Figure 4-12. By contrast, the bridge data suggest a slight decrease of ϵ_r', with frequency (curve B), or an independence of frequency (curve A of Figure 4-12). Figure 4-13 shows the variation of the loss tangent of granite with frequency. Here the three methods of measurement yield data that decrease with increasing frequency. Actually, the bridge method with coaxial sample holder generates data that can be roughly extrapolated to the data generated with the slotted-line (see curves B and C in Figure 4-13).

The slotted-line technique was also used to determine the dielectric parameters of a quartzite cylindrical sample with the same dimensions as those of basalt and granite. The data obtained with quartzite is shown in Table 4-7. In this case, the variation of ϵ_r' with frequency is shown in curve C of Figure 4-14. The data seem to rise to a maximum at about 1.5 GHz. It should also be noted that the measurements taken with the bridge method and the coaxial sample holder appear to be consistent with those determined by the slotted-line method (see curves B and C of Figure 4-11). The loss tangent of quartzite decreases steadily with frequency as shown in Figure 4-15, curves B and C. The data measured with the parallel-plate bridge method (curve A) appear to be unreliable. The points at 10 and 20 MHz depart considerably from those determined with the same technique at 40 and 70 MHz due to the bridge inaccuracy for high values of R_p ($R_p > 100K\Omega$).

Table 4-6. Dielectric Parameters of Granite. Slotted-Line Method

Granite: l_m = 10.17 cm; d_{out} = 14 mm, d_{in} = 6 mm; GR 874 Sample Holder; T = T_{ROOM} ≈ 22°C.
Assumed L_{SH} = 43.65 cm for each data point.

L_{MIN} (cm)	f_{RES} (GHz)	$\lambda_{o_{RES}}$ (cm)	$\lambda_o/2$ (cm)	k_m	$\left(\frac{\lambda_o}{2} \cdot \frac{k_m}{l_m}\right)^2 = \epsilon_r'$	Δl^* (cm)	Δl_o (cm)	$\Delta l^* - \Delta l_o = \Delta l$(cm)	α_o(nep/cm) x10^{-4}	$\frac{\Delta l}{\epsilon_r' l_m} - \frac{\lambda_o}{\pi} \alpha_o = \tan\delta$	ϵ_r''
37.83	0.315	95.25	47.6	0.5	5.49	1.7013	0.1230	1.5783	0.903	0.0283 - 0.0027 = 0.0256	0.141
16.50	0.601	49.9	24.95	1.0	6.03						
24.87	0.898	33.4	16.7	1.5	6.07	1.3986	0.0648	1.3338	1.386	0.02165 - 0.00147 = 0.02018	0.122
17.20	1.184	25.33	12.67	2.0	6.22						
12.10	1.48	20.27	10.14	2.5	6.21	1.3139	0.0440	1.228	1.69	0.01947 - 0.00109 = 0.01838	0.114
10.14	1.75	17.15	8.57	3.0	6.42						

Table 4-7. Dielectric Parameters of Quartzite. Slotted-Line Method

Quartzite: l_m = 10.15 cm; d_{out} = 14 mm, d_{in} = 6 mm; GR 874 Sample Holder; T = T_{ROOM} ≈ 22°C

Assumed L_{SH} = 43.65 cm for each data point.

L_{MIN} (cm)	f_{RES} (GHz)	$\lambda_{o_{RES}}$ (cm)	L_{SH} (cm)	$\lambda_o/2$ (cm)	k_m	$(\frac{\lambda_o}{2} \cdot \frac{k_m}{l_m})^2 = \epsilon_r'$	Δl^* (cm)	Δl_o (cm)	$\Delta l^* - \Delta l_o = \Delta l$(cm)	α_o(nep/cm) x10^{-4}	$\frac{\Delta l}{\epsilon_r' \ell_m}$	$- \frac{\lambda_o}{\pi} \alpha_o$	= tan δ	ϵ_r''
28.46	0.363	82.7	43.78	41.4	0.5	4.17	0.4030	0.1097	0.2933	0.947	0.00693	- 0.00249	= 0.00444	0.0185
29.00	0.720	41.7	43.82	20.85	1.0	4.21								
16.89	1.042	28.8	43.77	14.4	1.5	4.52	0.2701	0.0540	0.2161	1.48	0.00471	- 0.00471	= 0.00335	0.0151
10.90	1.350	22.2	43.67	11.1	2.0	4.57								
14.28	1.725	17.4	43.78	8.70	2.5	4.59	0.2310	0.0422	0.1888	1.794	0.00406	- 0.00099	= 0.00307	0.0141
9.15	2.11	14.23	43.71	7.12	3.0	4.42								

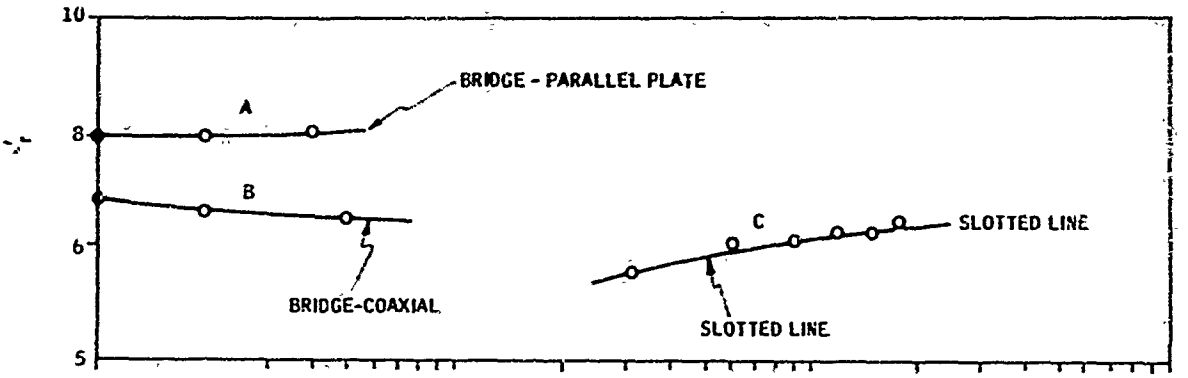

Figure 4-12. Relative Dielectric Constant of Granite in the Frequency Range 10 MHz to 2 GHz.

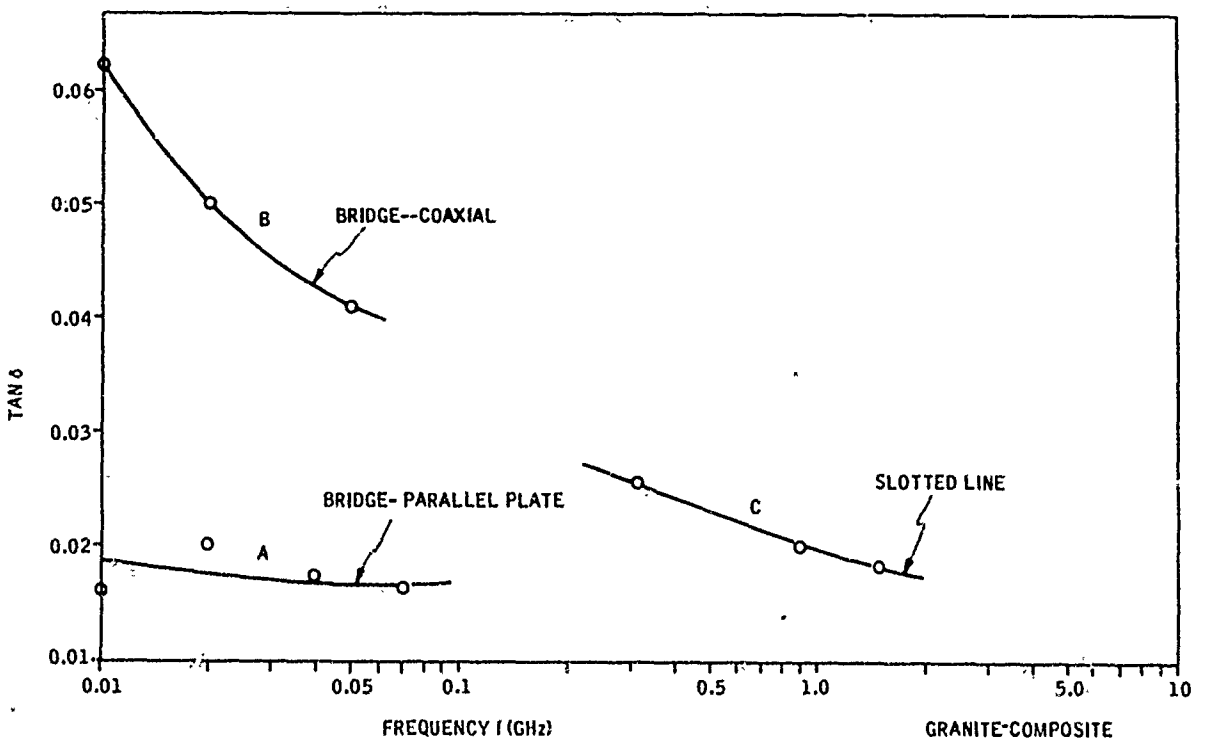

Figure 4-13. Loss Tangent of Granite in the Frequency Range 10 MHz to 2 GHz.

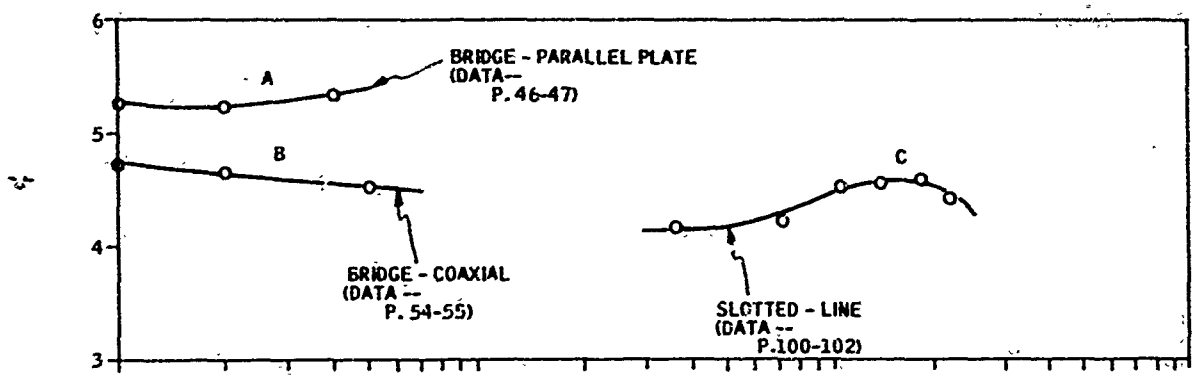

Figure 4-14. Relative Dielectric Constant of Quartzite in the Frequency Range 10 MHz to 2 GHz

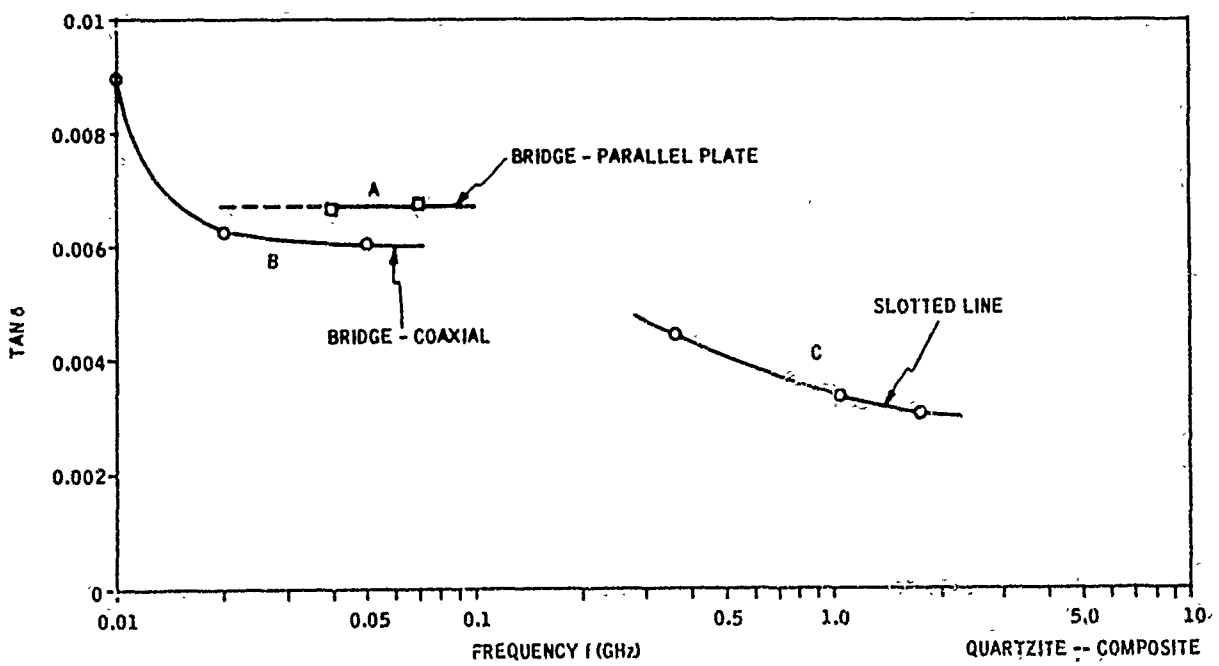

Figure 4-15. Loss Tangent of Quartzite in the Frequency Range 10 MHz to 2 GHz

SECTION V
EFFECT OF FREQUENCY ON ROCK DIELECTRIC PROPERTIES

The experimental data presented in Section IV suggest that one or possibly more of the techniques used to measure rock dielectric permittivity is giving the wrong answers. In general, the parallel-plate bridge method deviates from the bridge method with coaxial sample holder and also from the slotted-line method. The latter two methods appear to extrapolate with each other reasonably well, suggesting a continuity of the general trend of results obtained therefrom.

Theories of dielectric relaxation predict that both the real, ϵ_r', and the imaginary, ϵ_r'', parts of the relative complex permittivity should decrease with increasing frequency, provided that we are working at frequencies in excess of the turnover, or characteristic frequency of the system. The loss factor, $\tan \delta = \epsilon_r'' / \epsilon_r'$, is also theoretically expected to decrease with frequency since ϵ_r'' decreases much faster than ϵ_r' with frequency. This is because ϵ_r' approaches its value at infinite frequency, ϵ_∞', by linearly descending along the abscissa. Any increase in these dielectric parameters with frequency can only happen at frequencies less than the characteristic frequency. Except for data obtained with the parallel-plate bridge techniques at frequencies between 70 and 100 MHz, and for the ϵ_r' data of granite and quartzite with the slotted line, as well as $\tan \delta$ of basalt, the rest of the data shows the expected decrease in both ϵ_r' and $\tan \delta$ with increasing frequency. The rise in ϵ_r' and $\tan \delta$ above 70 MHz is most probably an error in the part of the parallel-plate bridge methods (see Figures 4-1 through 4-6). It is concluded from this limited amount of data that the bridge method with coaxial sample holder yields the most reliable rock permittivity data between 10 and 50 MHz, while the slotted line appears to give reliable information between 0.2 and 2 GHz.

Unlike the low-frequency spectra of rock electrical parameters, the present high-frequency data do not show any sign of dielectric dispersion, suggesting the absence of relaxation effects due to large structural units (e.g., silica tetrahedra, $[SiO_4]$ units or the presence of water in the rock) that would give a dispersion at frequencies lower than those investigated in this report.

Measurements on basalt indicate a general spectrum of relative dielectric constant of about 13.1 at 50 MHz to about 9.6 at 1 GHz, and loss tangent of 0.10 at 50 MHz to 0.056 at 1 GHz, with no frequency dispersion in either. Measurements on granite indicate a relative dielectric constant of about 6.5 at 50 MHz and 6.1 at 1 GHz, and a loss tangent of 0.042 and 0.02 at these two frequencies. Measurements on quartzite indicate a relative dielectric constant of about 4.5 at both 50 MHz and 1 GHz, and a loss tangent of 0.006 at 50 MHz decreasing to 0.0034 at 1 GHz.

The above numbers indicate that at a given frequency the relative dielectric constant of basalt is nearly twice that of granite and three times that of quartzite. The loss tangent of basalt is about three times that of granite and about fifteen times larger than that of quartzite. These trends can be correlated with the presence of ilmenite (mixed oxide of iron and titanium, $FeTiO_3$) in basalt, and its virtual absence from granite and quartzite. Chemical analysis of these three rock samples indicates that basalt, granite, and quartz contain 48.4, 63.5, and 97.8 percent silica and 6.2, 2, and 0.2 percent iron oxide (mostly FeO), respectively. Only basalt showed a measurable analysis of 1.9 percent Titania (TiO_2).

The dielectric permittivity of a system, which is an unordered mixture of two components, can be computed with the aid of Lichtenikers' formula (Ref. 3)

$$\log \epsilon_r' = \theta_1 \log \epsilon_1' + \theta_2 \log \epsilon_2' \qquad (5\text{-}1)$$

where ϵ_1' and ϵ_2' are the permittivities of the two components and θ_1 and θ_2 are their volume fractions. The above formula can also be written as

$$\epsilon_r' = \prod_i \epsilon_i'^{\theta_i} \tag{5-2}$$

When there is a large difference in the dielectric permittivities, Adelevskiis formula (Ref. 3) had been reported to give better results

$$\epsilon_r' = B + \sqrt{B^2 + \frac{\epsilon_1' \epsilon_2'}{2}} \tag{5-3}$$

where

$$B = \frac{(3\theta_1 - 1)\epsilon_1' + (3\theta_2 - 1)\epsilon_2'}{4} \tag{5-4}$$

The dielectric permittivity of TiO_2 is reported (Ref. 3) to be 78 (when present as brookite), and to vary between 89 and 173 when present as rutile. That of pure silica varies between 5.6 and 7.5. For magnetite, ϵ_r' is more than 33.7 and less than 81, and the same values are reported (Ref. 3) for ilmenite. The rest of the alkali metal oxides and alkaline earth oxides would have ϵ_r' values between 5 and 10. The densities of TiO_2, SiO_2, Fe_3O_4, $FeTiO_3$, and Na_2O, CaO are, respectively, 3.9 to 4.2, 2.5 to 2.6, 4.9 to 5.2, 4.4 to 5, and 1 to 3 gm cm^{-3}.

SECTION VI
ROCK DIELECTRIC PROPERTIES AT ELEVATED TEMPERATURES

The objective of this phase of the investigation was to determine how the relative dielectric constant (ϵ_r'), the relative dielectric loss (ϵ_r''), and the loss tangent (tan δ) change with temperature at a fixed frequency. Slotted-line measurements were first made at a nominal frequency of 1.15 GHz on a basaltic rock cylinder of length ℓ_m = 10.16 cm, d_{out} = 14 mm, and d_{in} = 6 mm; the measurement data are presented in Table 6-1.

Table 6-1. Effect of Temperature on Dielectric Properties of Basalt at 1.15 GHz

Temperature (°C)	L_{min} (cm)	λ_o (cm)	f_{res} (GHz)	ϵ_r'*	$\alpha_o \times 10^{-4}$ (Nep/cm)	Tan δ**	ϵ_r''	$\frac{1000}{T}$ (°K^{-1})
24	10.72	25.24	1.188	9.67	1.556	0.0501	0.484	3.37
50	10.86	25.32	1.184	9.72	1.554	0.0554	0.539	3.10
100	11.81	25.89	1.158	10.14	1.542	0.0606	0.615	2.68
150	12.82	26.48	1.132	10.63	1.528	0.0677	0.721	2.36
200	***							2.11
250	***							1.91

* $\epsilon_r' = \left(\frac{\lambda_o}{2} \quad \frac{k_m}{\ell_m}\right)^2$

** $\text{Tan } \delta = \frac{\Delta L}{\epsilon_r \ell_m} - \frac{\lambda_o}{\pi} \alpha_o$

***No resonance was possible.

Because of the difficulty of obtaining resonance at 1.15 GHz and at temperatures above 150°C, measurements were repeated on basalt at a nominal frequency of 0.69 GHz; results are presented in Table 6-2.

Table 6-2. Effect of Temperature on the Dielectric Properties of Basalt at 0.69 GHz

Temperature (°C)	L_{min} (cm)	λ_o (cm)	f_{res} (GHz)	ϵ_r'*	$\alpha_o \times 10^{-4}$ (Nep/cm)	Tan δ**	ϵ_r''	$\frac{1000}{T}$ (K^{-1})
25	12.56	42.43	0.707	9.86	1.24	0.0485	0.478	3.37
50	12.76	42.76	0.702	9.96	1.23	0.0538	0.536	3.10
100	20.30	43.26	0.694	10.20	1.23	0.0598	0.610	2.68
150	21.04	43.79	0.685	10.45	1.22	0.0732	0.765	2.36
200	21.66	44.28	0.678	10.68	1.22	0.0812	0.867	2.11
250	21.95	44.53	0.674	10.80	1.21	0.0912	0.985	1.91
300	22.14	44.70	0.672	10.89	1.21	0.1021	1.113	1.75

*$\epsilon_r' = \left(\frac{\lambda_o}{2} \frac{k_m}{t_m}\right)^2$

**$\text{Tan } \delta = \frac{\Delta L}{\epsilon_r t_m} - \frac{\lambda_o}{\pi} \alpha_o$

The variation of the relative dielectric constant and the loss tangent of Dresser basalt with temperature is illustrated in Figures 6-1 and 6-2.

The effect of temperature on the dielectric parameters of granite was also investigated. Following the basalt tests, the sample holder was cleaned with crocus cloth and cleaning fluid. Molybdenum disulfide was also put on the screw threads to prevent their seizure by exposure to high temperature. The results obtained with a granite cylindrical rock sample of length 10.17 cm are shown in Table 6-3.

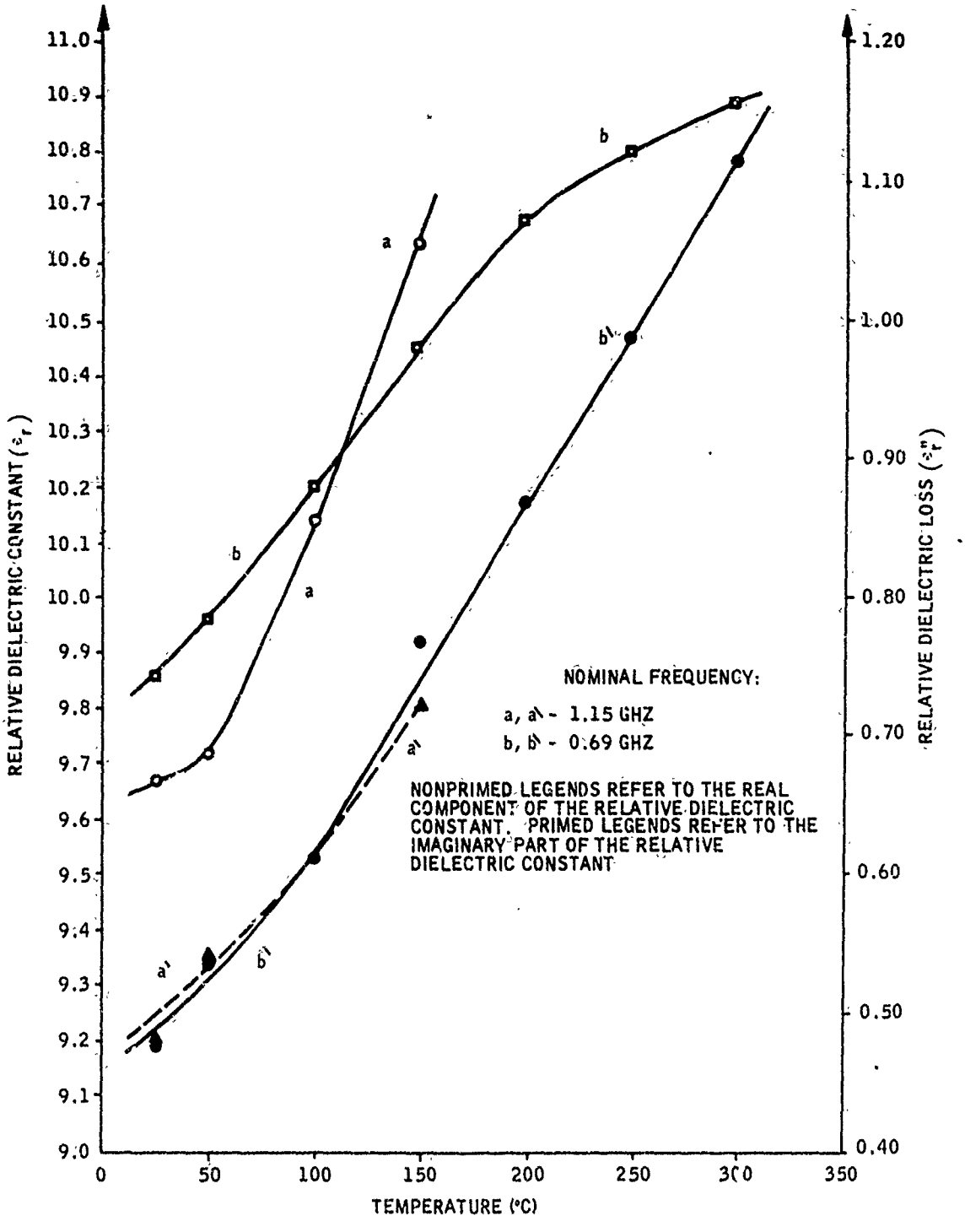

Figure 6-1. Variation with Temperature of Basalt's Relative Dielectric Constant and Dielectric Loss at Two Frequencies

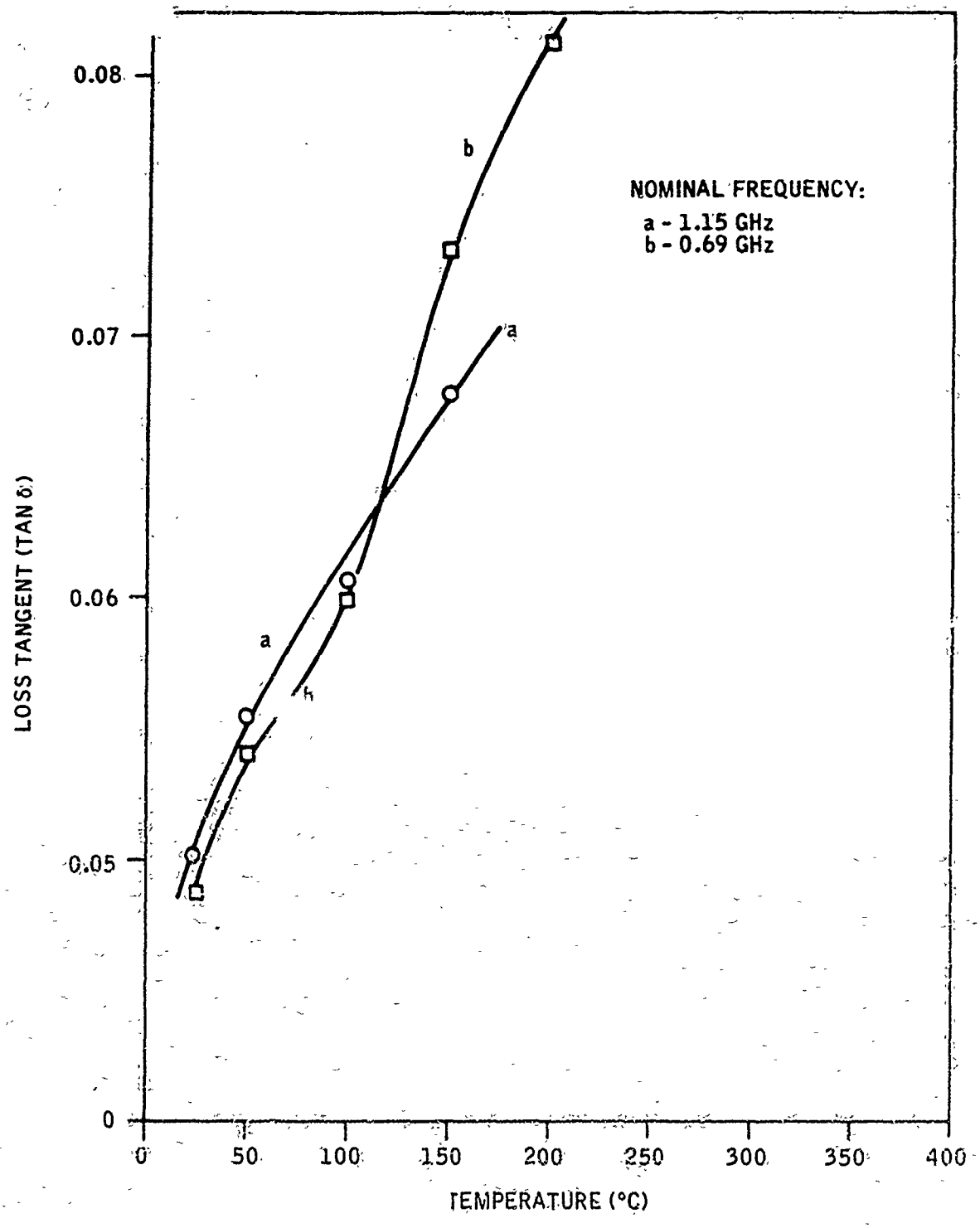

Figure 6-2. Variation of Basalt's Loss Tangent With Temperature

Table 6-3. Effect of Temperature on the Dielectric Properties of Granite at 1.50 GHz

Temperature (°C)	L_{min} (cm)	λ_o (cm)	f_{res} (GHz)	ϵ_r'*	$\alpha_o \times 10^{-4}$ (Nep/cm)	Tan δ**	ϵ_r''	$\frac{1000}{T}$ (°K^{-1})
24	11.32	19.96	1.503	6.03	1.66	0.0173	0.104	3.37
50	11.42	20.00	1.500	6.05	1.66	0.0198	0.120	3.10
100	11.61	20.08	1.494	6.10	1.66	0.0221	0.135	2.68
150	11.72	20.14	1.489	6.14	1.66	0.0240	0.147	2.36
200	11.86	20.19	1.486	6.16	1.66	0.0276	0.170	2.11
250	11.88	20.20	1.485	6.17	1.66	0.0294	0.181	1.91
300	11.89	20.21	1.485	6.18	1.66	0.0307	0.190	1.75
350	12.01	20.26	1.480	6.20	1.66	0.0345	0.214	1.61
400	12.04	20.27	1.479	6.22	1.66	0.0351	0.218	1.49
450	12.16	20.33	1.477	6.25	1.66	0.0365	0.228	1.38

*$\epsilon_r' = \left(\frac{\lambda_o}{2} \quad \frac{k_m}{\ell_m}\right)^2$

**Tan $\delta = \frac{\Delta L}{\epsilon_r \ell_m} - \frac{\lambda_o}{\pi} \alpha_o$

The variation of ϵ_r' and ϵ_r'' of granite with temperature is shown in Figure 6-3. The effect of temperature on the loss tangent of granite is shown in Figure 6-4.

The high-temperature dielectric properties of quartzite were determined following a clean-up of the sample holder from the previous measurements on granite. The same procedure of sample holder clean-up and screw thread treatment was repeated as was performed before measurements on granite were taken. The experimental data recorded on a quartzite cylindrical rock sample of length 9.644 cm are given in Table 6-4.

The variation of the relative dielectric constant of quartzite with temperature is shown in Figure 6-5. The change of quartzite loss tangent with temperature is shown in Figure 6-6. In the previous two rocks of basalt and granite, the loss tangent increased with temperature rise. In the case of quartzite, the loss tangent exhibits a minimal value of 4.37×10^{-3} at 100°C. Simultaneously, the relative dielectric loss of quartzite exhibits on minimal value of 2.04×10^{-2} at 100°C. Because the relative dielectric loss is directly linked to the rock conductivity, it appears that two mechanisms are operative in the electrical conductance of quartzite. The electrolytic mechanism contributes a conductivity that increases with increasing water content in the rock micropores. Upon heating the rock, the water is driven off and the contribution to rock conductivity by the electrolytic mechanism is reduced. The other mechanism responsible for electric conductance in rock is the ionic-pump mechanism. Here, ionic constituents of the lattice are the mobile particles that diffuse either interstitially or by a vacancy mechanism. This type of conductance increases with temperature rise and often follows an exponential increase. Section VIII contains a theoretical treatment of the ionic conductivity in rocks. The combined effect of temperature on the two types of conductance, one decreasing and the other increasing with temperature rise, can explain the occurrence of a minimum in Figure 6-6.

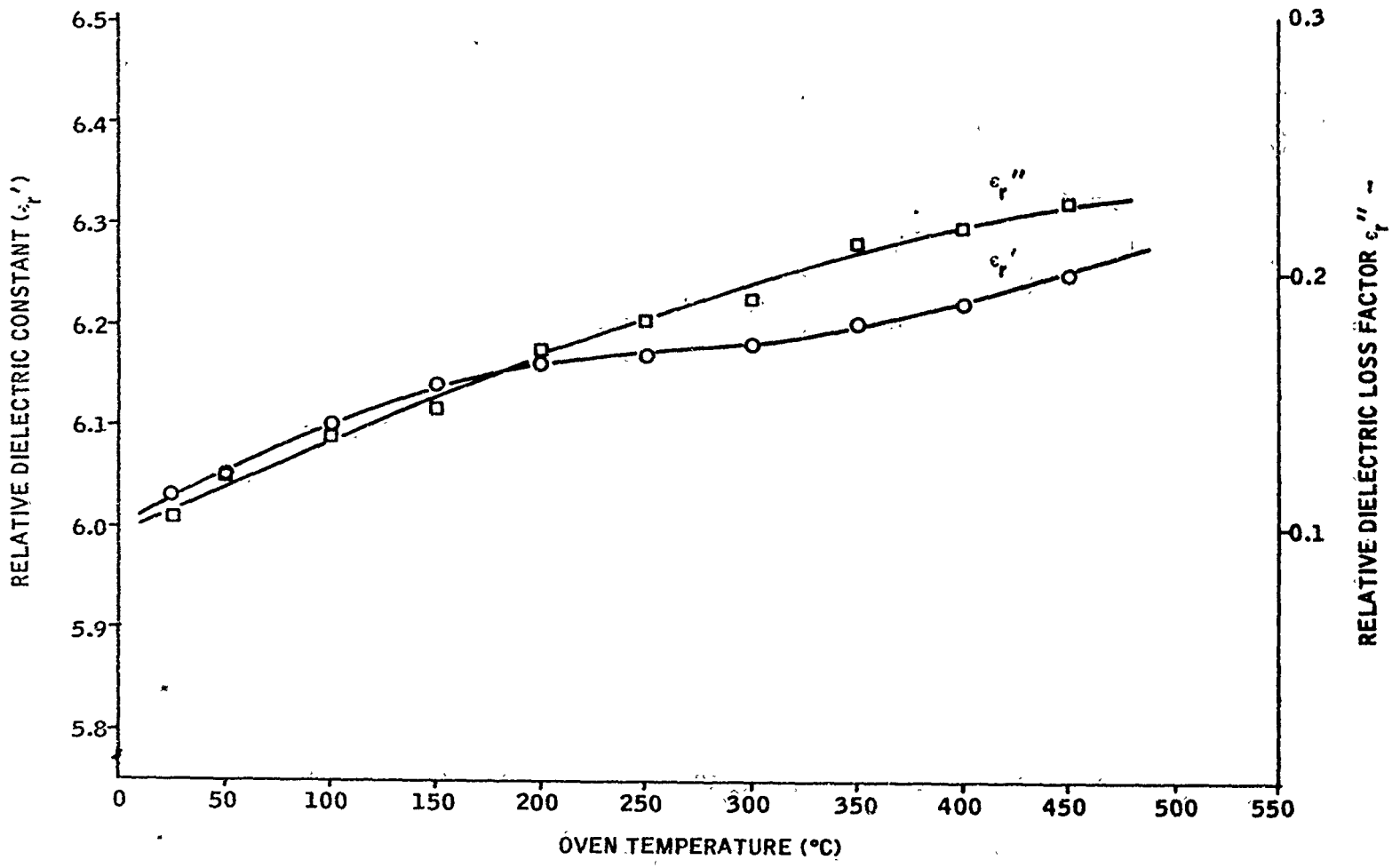

Figure 6-3. Effect of Temperature on the Relative Dielectric Constant and the Relative Dielectric Loss of Granite at a Nominal Frequency of 1.5 GHz

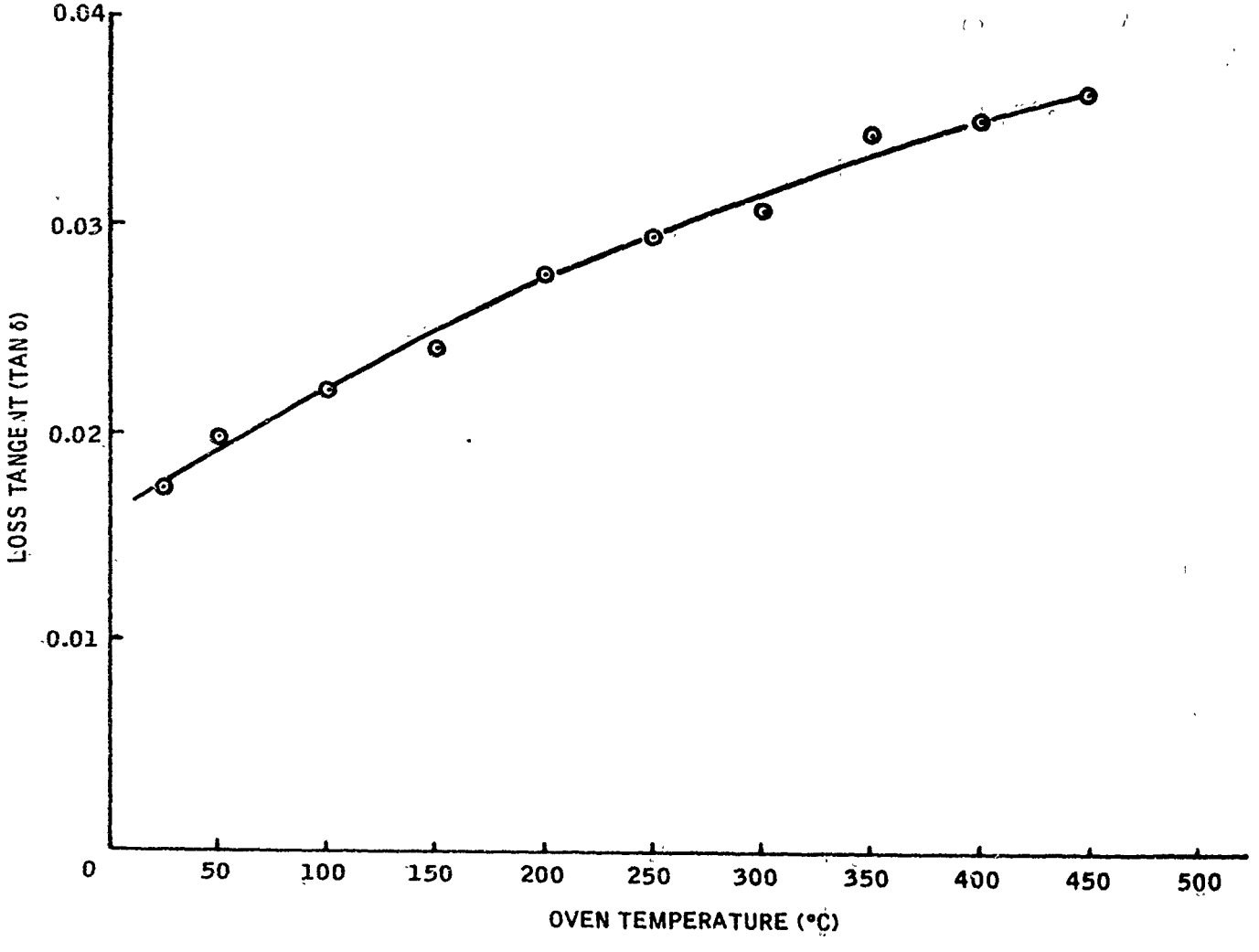

Figure 6-4. Effect of Temperature on the Loss Tangent of Granite at a Nominal Frequency of 1.5 GHz

Table 6-4. Effect of Temperature on the Dielectric Properties of Quartzite at a Nominal Frequency of 1.80 GHz

Temperature (°C)	L_{min} (cm)	λ_o (cm)	f_{res} (GHz)	ε_r'*	$\alpha_o \times 10^{-4}$ (Nep/cm)	Tan δ**	ε_r''	$\frac{1000}{T}$ (°K^{-1})
25	11.52	16.60	1.807	4.63	1.825	0.00455	0.0211	3.37
50	11.65	16.64	1.803	4.65	1.824	0.00443	0.0206	3.10
100	11.69	16.66	1.801	4.66	1.822	0.00437	0.0204	2.68
150	11.80	16.70	1.796	4.68	1.820	0.00468	0.0219	2.36
200	11.90	16.74	1.792	4.71	1.820	0.00510	0.0240	2.11
250	12.00	16.78	1.787	4.73	1.818	0.00600	0.0284	1.91
300	12.14	16.83	1.781	4.76	1.815	0.01009	0.0479	1.75

$$*\varepsilon_r' = \left(\frac{\lambda_o}{2}\ \frac{k_m}{\ell_m}\right)^2$$

$$**\text{Tan } \delta = \frac{\Delta L}{\varepsilon_r \ell_m} - \frac{\lambda_o}{\pi}\ \alpha_o$$

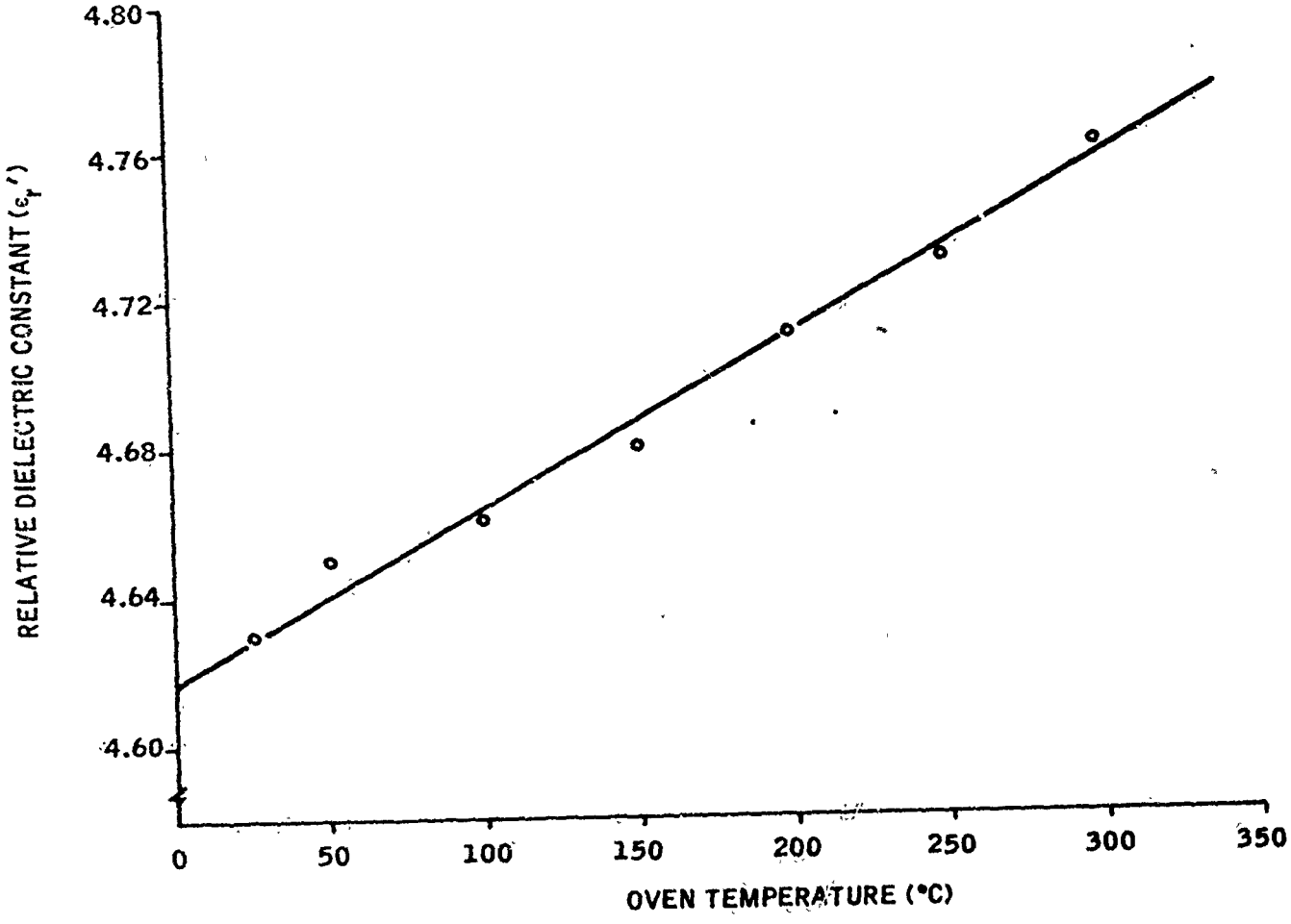

Figure 6-5. Effect of Temperature on the Relative Dielectric Constant of Quartzite at a Nominal Frequency of 1.80 GHz

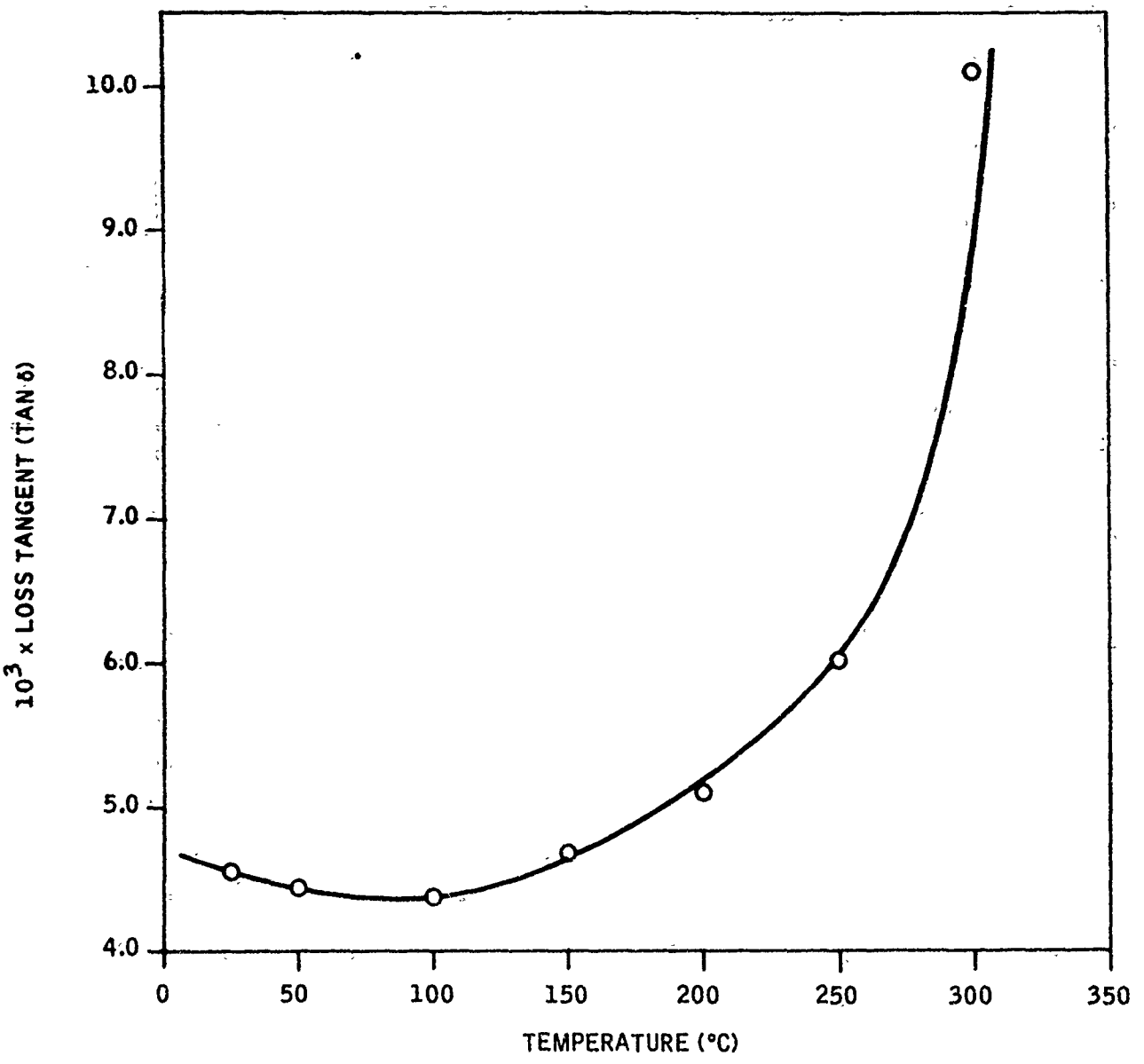

Figure 6-6. Effect of Temperature on the Relative Dielectric Loss Tangent of Quartzite at a Nominal Frequency of 1.80 GHz

SECTION VII
EFFECT OF TEMPERATURE ON ROCK DIELECTRIC PERMITTIVITY

Dielectric measurements on rocks at various temperatures can reveal a host of rock thermophysical and mechanical properties. Because of the complex structure of rocks, we followed the recommendation of Huggins (Ref. 4) in using local structural groupings as the basic structural units in rocks. The term structon was used to signify a specific type of atom with specific kinds and numbers of close neighbors.

The relationship between polarizability (α) and the relative dielectric permittivity (ϵ_r') is given for simple systems by the Clausius-Mosotti equation (Ref. 5) as

$$\frac{\epsilon_r' - 1}{\epsilon_r' + 2} = \frac{4\pi}{3} n\alpha \qquad (7\text{-}1)$$

where n is the number of particles per unit volume. The total polarizability (α) is sometimes regarded as equal to the sum of electronic (α_e) plus atomic (α_a) plus molecular or orientational (α_m) polarizabilities. In general, α_e and α_a are temperature insensitive. Unless the number density of elementary particles shows a significant decrease with rise in temperature (as in gases or liquids), the change with temperature of ϵ_r' due to electronic or atomic polarizations will be overshadowed by the large changes in orientation polarization. Orientation of dipoles in an applied electric field will depend on temperature, complete orientation prevented by thermal agitation. Polarizability under these conditions will decrease with rise of temperature according to

$$\alpha_m = \mu^2/3kT \qquad (7\text{-}2)$$

where μ is the electric moment of the polar group in the molecule, k is Boltzmann's constant, and T is the absolute temperature. In the presence of polar molecules, the Clausius-Mosotti relation was amended by Debye (Ref. 5) in the form

$$\frac{\epsilon_r' - 1}{\epsilon_r' + 2} = \frac{4\pi}{3} n \left[\alpha_s + \frac{\mu^2}{3kT}\right] \tag{7-3}$$

where α_s now refers to the structural polarizability, equal to $(\alpha_e + \alpha_a)$. In this form, physical chemists have extensively used Equation (7-3) to elucidate molecular structure and molecular dipole moments.

In the absence of permanent dipole moments (i.e., when $\mu = 0$), we applied the Clausius-Mosotti relations for rocks in the form

$$\frac{\epsilon' - 1}{\epsilon' + 2} = \frac{4\pi}{3} n \alpha_s = \frac{4\pi}{3} \varphi \tag{7-4}$$

where n is now the number of rock structons per unit volume and α_s is the structon's polarizability, equal to the cube of its average radius (assumed spherical). The product $n\alpha_s$ may, therefore, be regarded as the true volume, φ, of the solid rock, excluding the pores, fractures, or solid imperfections, whose addition to φ gives V, the total or apparent rock volume. Upon differentiating Equation (7-4) with respect to temperature at constant pressure, one obtains

$$\left\{ \frac{1}{\epsilon_r' - 1} - \frac{1}{\epsilon_r' + 2} \right\} \frac{\delta \epsilon_r'}{\delta T} = \frac{1}{\varphi} \left| \frac{\delta \varphi}{\delta T} \right| = \beta \tag{7-5}$$

or

$$\beta = \frac{3}{(\epsilon_r' - 1)(\epsilon_r' + 2)} \left| \frac{\delta \epsilon}{\delta T} \right| \tag{7-6}$$

where β is the isobarric coefficient of volume expansion. In the present investigation, Equation (7-6) was used for the first time to evaluate the coefficient of thermal expansion for the three representative rock samples (Dresser basalt, charcoal granite, and Sioux quartzite).

The dielectric data obtained with basalt at a nominal frequency of 0.69 GHz in the temperature range 25 to 300°C are shown in Table 7-1. The estimated coefficient of thermal expansion is listed at each temperature in the third column of that table.

Table 7-1. Effect of Temperature on the Th mal Expansion Coefficient of Basalt

Temperature (°C)	ϵ_r'	$\beta \times 10^4$ ($°C^{-1}$)
25	9.86	1.03
50	9.96	1.18
100	10.20	1.31
150	10.45	1.22
200	10.68	0.85
250	10.80	0.57
300	10.92	0.56

The granite dielectric data measured at a nominal frequency of 1.50 GHz were also used to estimate the thermal expansion coefficient of that rock; the results are given in Table 7-2.

The relative dielectric constants of quartzite at a nominal frequency of 1.80 GHz were also used to estimate the thermal expansion coefficient of that rock. The data obtained at various temperatures are shown in Table 7-3.

Table 7-2. Effect of Temperature on the Thermal Expansion Coefficient of Granite

Temperature (°C)	ϵ_r'	$\beta \times 10^5$ ($°C^{-1}$)
25	6.03	5.2
50	6.05	6.3
100	6.10	6.5
150	6.14	4.3
200	6.16	2.1
250	6.17	1.4
300	6.18	2.1
350	6.20	2.8
400	6.22	3.5
450	6.25	4.8

Table 7-3. Effect of Temperature on the Thermal Expansion Coefficient of Quartzite

Temperature (°C)	ϵ_r'	$\beta \times 10^5$ ($°C^{-1}$)
25	4.63	5.8
50	4.65	8.0
100	4.66	7.3
150	4.68	6.1
200	4.71	6.0
250	4.73	6.0
300	4.76	5.9

The thermal expansion coefficient is a complex function of temperature. The variation of this coefficient with temperature is illustrated in Figure 7-1 for the three rocks investigated. For basalt, the thermal expansion coefficient exhibits a maximum of $1.31 \times 10^{-4}\ °C^{-1}$ at about 100°C. For quartzite, a maximum in β is estimated as $8.5 \times 10^{-5}\ °C^{-1}$ at about 70°C. For granite, β shows a maximum value of $6.7 \times 10^{-5}\ °C^{-1}$ at about 80°C.

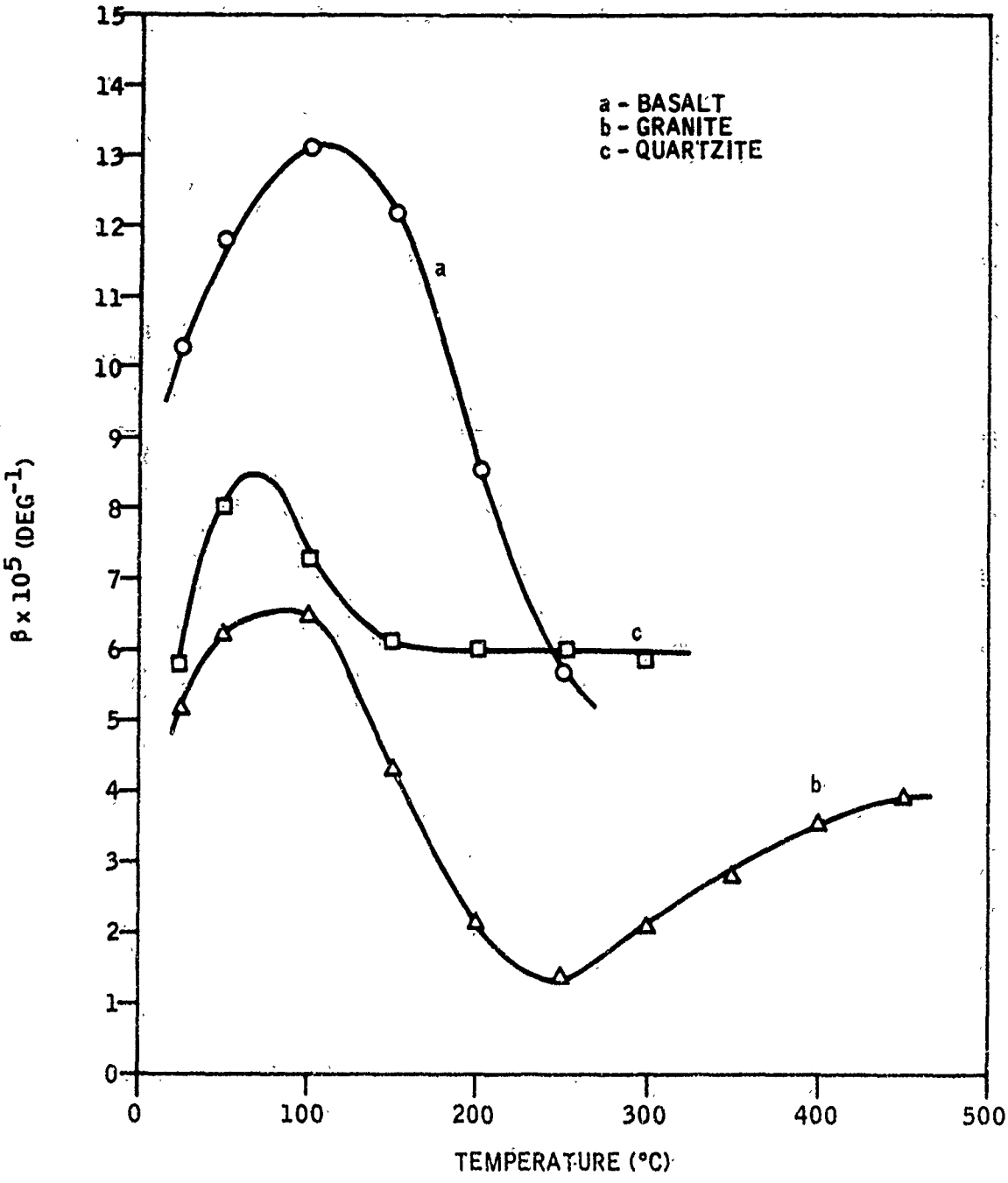

Figure 7-1. Variation of the Rock Thermal Expansion Coefficient with Temperature

SECTION VIII

EFFECT OF TEMPERATURE ON THE RELATIVE DIELECTRIC LOSS

The relative dielectric loss is expected to follow an Arrhenius type of dependence on temperature. This is because dielectric loss is interrelated with electric conductance, σ, according to

$$\sigma = \omega\epsilon'' = \omega\epsilon_o \epsilon_r'' \tag{8-1}$$

where ω is the angular frequency, ϵ'' is the imaginary component of the dielectric permittivity, and ϵ_o is the permittivity of free space.

The variation of the conductivity, σ, of solid minerals in a rock with temperature is often given by

$$\sigma_t = \sigma_o e^{-Q/2kT} \tag{8-2}$$

where Q is an activation energy. Equation (8-2) is valid when the minerals are electron semiconductors. When the minerals in the rock are dielectric insulators, then the conductivity variation with temperature becomes

$$\sigma_t = \sigma_o e^{-Q/kt} \tag{8-3}$$

In either case, the conductivity will increase, and the resistivity will decrease with a rise in temperature. The plot of $\ell_n\, \sigma_t$ with the reciprocal of absolute temperature, $\frac{1}{T}$, will, in a well-behaved system, give a straight line whose slope is $-\frac{Q}{k}$ for dielectric insulators and $-\frac{Q}{2k}$ for semiconductors.

At subzero temperatures, Parkhomenko (Ref. 3) was able to draw the following general conclusions from the experimental data available on rocks

- A pronounced change in resistivity as a function of temperature is associated with the freezing or thawing of an electrolyte in the pores of a rock.

- The actual resistivity at low temperatures depends on the water content, the chemical composition of the electrolyte, and the grain size of the rock.

- The resistivity of fine-grained rocks (shale) increases less abruptly with decreasing temperature than does the resistivity of coarse-grained rocks.

- With increasing salinity of the pore water, the increase in resistivity on freezing is reduced. Data on the relationship between resistivity and ice content at freezing temperatures may be used in interpreting electrical geophysical surveys made in permafrost areas.

Resistivity of water-bearing rocks will result from the combined effects of its liquid and solid fractions. The resistivity of electrolytes decreases, and, hence, its conductivity increases with a temperature rise.

The temperature coefficient of the conductivity of most electrolytes averages about 2.5 percent per degree centigrade. The value of this coefficient increases with decreasing salinity. Because sedimentary rocks lie in the upper part of the earth's crust (where the temperatures do not exceed 200 to 250°C), a decrease in resistivity with depth caused by the decrease in the resistivity of the pore water with temperature is observed.

When the rise in temperature causes an evolution of water from the rock, the resistivity will change anomalously. Studies of the temperature-resistivity curve for various types of coal, as well as for various rocks under laboratory conditions indicate that evolution of water is accompanied by a characteristic change in resistivity. The greater the original water content of a rock, the greater will be the anomalous rise in the resistivity on evolution.

In dry rocks without fractures, the relationship between resistivity and temperature is well described by Equation (8-3). When the log σ versus $\frac{1}{T}$ curve has a change in slope, an expression containing two exponential terms would fit the results

$$\sigma_t = \sigma_1 e^{-\frac{Q_1}{kT}} + \sigma_2 e^{-\frac{Q_2}{kT}} \qquad (8\text{-}4)$$

This corresponds to two mechanisms of conduction with two activation energies in the low- and high-temperature ranges.

Calculations of the rock conductivity from the previously determined relative dielectric losses (Section VI) were made. The results for basalt are given in Table 8-1.

Table 8-1. Electric Conductivity of Basalt at Various Temperatures

Temperature (°C)	$\frac{1000}{T}$ (°K^{-1})	f (GHz)	$\omega = 2\pi f$ (rad/sec)	ϵ_r''	$\epsilon'' = \epsilon_o \epsilon_r''$* (farad/meter)	$\sigma = \omega\epsilon''$ (ohm · meter)$^{-1}$
24	3.37	1.188	7.464×10^9	0.484	4.28×10^{-12}	3.19×10^{-2}
50	3.10	1.184	7.439×10^9	0.539	4.77×10^{-12}	3.55×10^{-2}
100	2.68	1.158	7.276×10^9	0.615	5.44×10^{-12}	3.96×10^{-2}
150	2.36	1.132	7.112×10^9	0.721	6.38×10^{-12}	4.54×10^{-2}

*$\epsilon_o = 8.85 \times 10^{-12}$ farad/meter.

Similar calculations of the granite and quartzite electric conductivity are given in Tables 8-2 and 8-3, respectively.

Table 8-2. Electric Conductivity of Granite at Various Temperatures

Temperature (°C)	$\frac{1000}{T}$ ($°K^{-1}$)	f (GHz)	$\omega = 2\pi f$ (rad/sec)	ϵ_r''	$\epsilon'' = \epsilon_o \epsilon_r''$ (farad/meter)	$\sigma = \omega \epsilon''$ (ohm-meter)$^{-1}$
25	3.37	1.503	9.443×10^9	0.104	9.20×10^{-13}	8.69×10^{-3}
50	3.10	1.500	9.424×10^9	0.120	1.06×10^{-12}	9.99×10^{-3}
100	2.68	1.494	9.387×10^9	0.135	1.19×10^{-12}	1.12×10^{-2}
150	2.36	1.489	9.355×10^9	0.147	1.30×10^{-12}	1.22×10^{-2}
200	2.11	1.486	9.337×10^9	0.170	1.50×10^{-12}	1.40×10^{-2}
250	1.91	1.485	9.330×10^9	0.181	1.60×10^{-12}	1.49×10^{-2}
300	1.75	1.485	9.330×10^9	0.190	1.68×10^{-12}	1.57×10^{-2}
350	1.61	1.480	9.299×10^9	0.214	1.89×10^{-12}	1.76×10^{-2}
400	1.49	1.479	9.293×10^9	0.218	1.92×10^{-12}	1.78×10^{-2}
450	1.38	1.477	9.280×10^9	0.228	2.02×10^{-12}	1.87×10^{-2}

Table 8-3. Electric Conductivity of Quartzite at Various Temperatures

Temperature (°C)	$\frac{1000}{T}$ ($°K^{-1}$)	f (GHz)	$\omega = 2\pi f$ (rad/sec)	ϵ_r''	$\epsilon'' = \epsilon_o \epsilon_r''$ (farad/meter)	$\sigma = \omega \epsilon''$ $(ohm \cdot meter)^{-1}$
25	3.37	1.807	1.135×10^{10}	0.0211	1.86×10^{-13}	2.11×10^{-3}
50	3.10	1.803	1.133×10^{10}	0.0206	1.82×10^{-13}	2.06×10^{-3}
100	2.68	1.801	1.132×10^{10}	0.0204	1.81×10^{-13}	2.05×10^{-3}
150	2.36	1.796	1.128×10^{10}	0.0219	1.94×10^{-13}	2.19×10^{-3}
200	2.11	1.792	1.126×10^{10}	0.0240	2.12×10^{-13}	2.39×10^{-3}
250	1.91	1.787	1.123×10^{10}	0.0284	2.51×10^{-13}	2.81×10^{-3}
300	1.75	1.781	1.119×10^{10}	0.0479	4.24×10^{-13}	4.74×10^{-3}

The previously determined dielectric loss data (Section VI) for basalt at a nominal frequency of 0.69 GHz were also used to calculate the electric conductivity of that rock at that frequency. These calculations are shown in Table 8-4.

Table 8-4. Electric Conductivity of Basalt at Various Temperatures Nominal Frequency = 0.69 GHz

Temperature (°C)	$\frac{1000}{T}$ ($°K^{-1}$)	f (GHz)	$\omega = 2\pi f$ (rad/sec)	ϵ_r''	$\epsilon'' = \epsilon_o \epsilon_r''$ (farad/meter)	$\sigma = \omega \epsilon''$ $(ohm \cdot meter)^{-1}$
25	3.35	0.707	4.44×10^{9}	0.478	4.23×10^{-12}	1.88×10^{-2}
50	3.10	0.702	4.41×10^{9}	0.536	4.74×10^{-12}	2.09×10^{-2}
100	2.68	0.694	4.36×10^{9}	0.610	5.40×10^{-12}	2.35×10^{-2}
150	2.36	0.685	4.30×10^{9}	0.765	6.77×10^{-12}	2.91×10^{-2}
200	2.11	0.678	4.26×10^{9}	0.867	7.67×10^{-12}	3.27×10^{-2}
250	1.91	0.674	4.23×10^{9}	0.985	8.72×10^{-12}	3.69×10^{-2}
300	1.75	0.670	4.21×10^{9}	1.113	9.85×10^{-12}	4.14×10^{-2}

The variation of the logorithm of the electric conductivity of basalt with the reciprocal absolute temperature is shown in Figure 8-1. At a nominal frequency of 1.15 GHz, the conductivity data are best fitted by the Arrhenius line (a) whose slope indicates an activation energy (Q) of 665 cal/mole or 2.88×10^{-2} ev. At a nominal frequency of 0.69 GHz, the data are fitted on two Arrhenius lines. The low-temperature line (b) is closely parallel to line (a) and indicates an activation energy of 660 cal/mole or 2.86×10^{-2} ev below 100°C.

Above 150°C, the basalt electric conductivity data fall on Arrhenius line b_2, which indicates an activation energy of 1.109 kcal/mole or 4.81×10^{-2} ev.

The foregoing experimental data on basalt at the lower frequency of 0.69 GHz are best explained by Equation (8-4) given in Parkhomenko monograph (Ref. 3).

$$\sigma_t = \sigma_1 e^{-Q_1/kT} + \sigma_2 e^{-Q_2/kT} \qquad (8-4)$$

where Q_1 and Q_2 are the activation energies corresponding to a low and a high temperature conduction mechanism. Experimentally, it was difficult to achieve resonance conditions with basalt in the slotted line at the higher frequency of 1.15 GHz when the rock temperature was 200°C and above (refer to Table 6-1). Because the relative dielectric loss (ϵ_r'') increases with frequency, increasing both frequency and temperature may render the dielectric properties of the relatively conducting basalt difficult to measure in slotted lines. Hence, no data can be obtained with the present equipment to support the high-temperature conduction mechanism for basalt at the higher frequency of 1.15 GHz. It is gratifying, however, to note that the activation energy at the low-temperature range is independent of the operating frequency as seen by the close parallelism of lines a and b_1 in Figure 8-1. It may be concluded, therefore, that the conduction mechanism in rocks, and hence the activation energy (Q), does not depend on the operating frequency, but can significantly depend on the temperature range at which

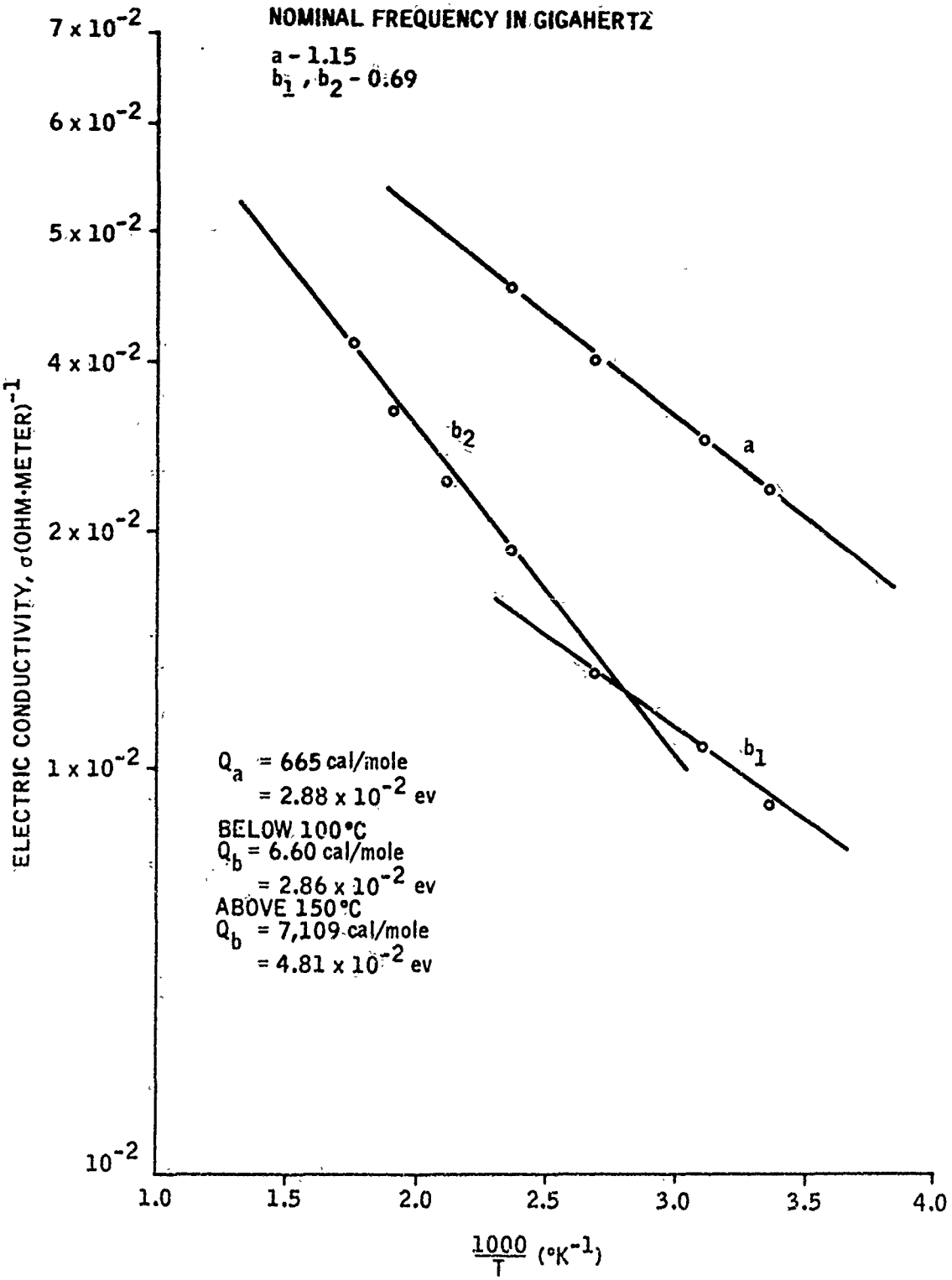

Figure 8-1. Arrhenius Plot of Basalt's Electric Conductivity

measurements are taken. More experimental work is needed to support or refute this seemingly logical conclusion.

The Arrhenius diagram for the electric conductivity data of granite at a nominal frequency of 1.5 GHz is shown in Figure 8-2. Here the data fit a single straight line in the temperature range 25° to 450°C. The slope of the line indicates an activation energy of 756 cal/mole or 3.28×10^{-2} ev. The granite rock is about 75 percent less conductive than basalt, and hence dielectric measurements were possible at the high frequency of 1.5 GHz and temperatures up to 450°C.

The electric conductivity data of quartzite did not fit to the Arrhenius diagram (Figure 8-3), but exhibit a minimum conductivity of about 2×10^{-3} $(\text{ohm} \cdot \text{meter})^{-1}$ at about 100°C. This anomalous change of conductivity with temperature has been shown by Parkhomenko (Ref. 3) to be caused by an evolution of water from the rock. The greater the original water content of a rock, the greater will be the anomalous rise in the resistivity (or fall in conductivity) with rise in temperature (or upon water evolution).

In a solid lattice, like that of rocks, the conducting particles and vacancies (or the electrons and holes in semiconductors) will migrate with a time average velocity $\langle \vec{V} \rangle$, which is to a good approximation proportional to the field, $\vec{E}$, if $|E|$ is not too large. The electric mobility, μ, is defined (Ref. 6) by

$$\langle \vec{V} \rangle = \pm \mu \vec{E} \tag{8-5}$$

The positive sign in Equation (8-5) applies for positively charged particles (or anion vacancies, or holes), and the negative sign applies for negatively charged particles (or cation vacancies, or electrons). Equation (8-5) is a simple representation of linear relations between components of vectors, with the mobilities represented by symmetric tensors.

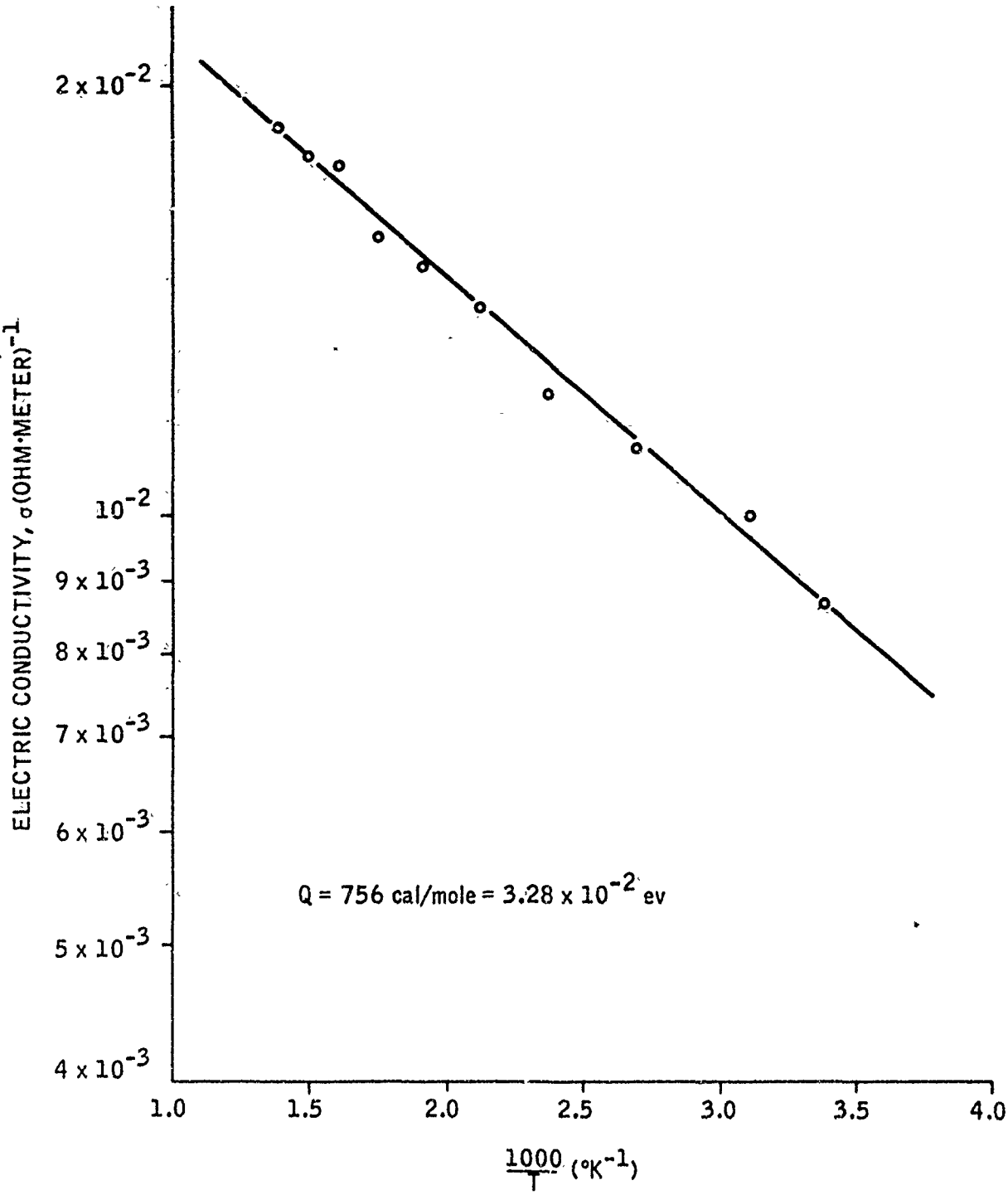

Figure 8-2. Arrhenius Plot of the Electric Conductivity of Granite

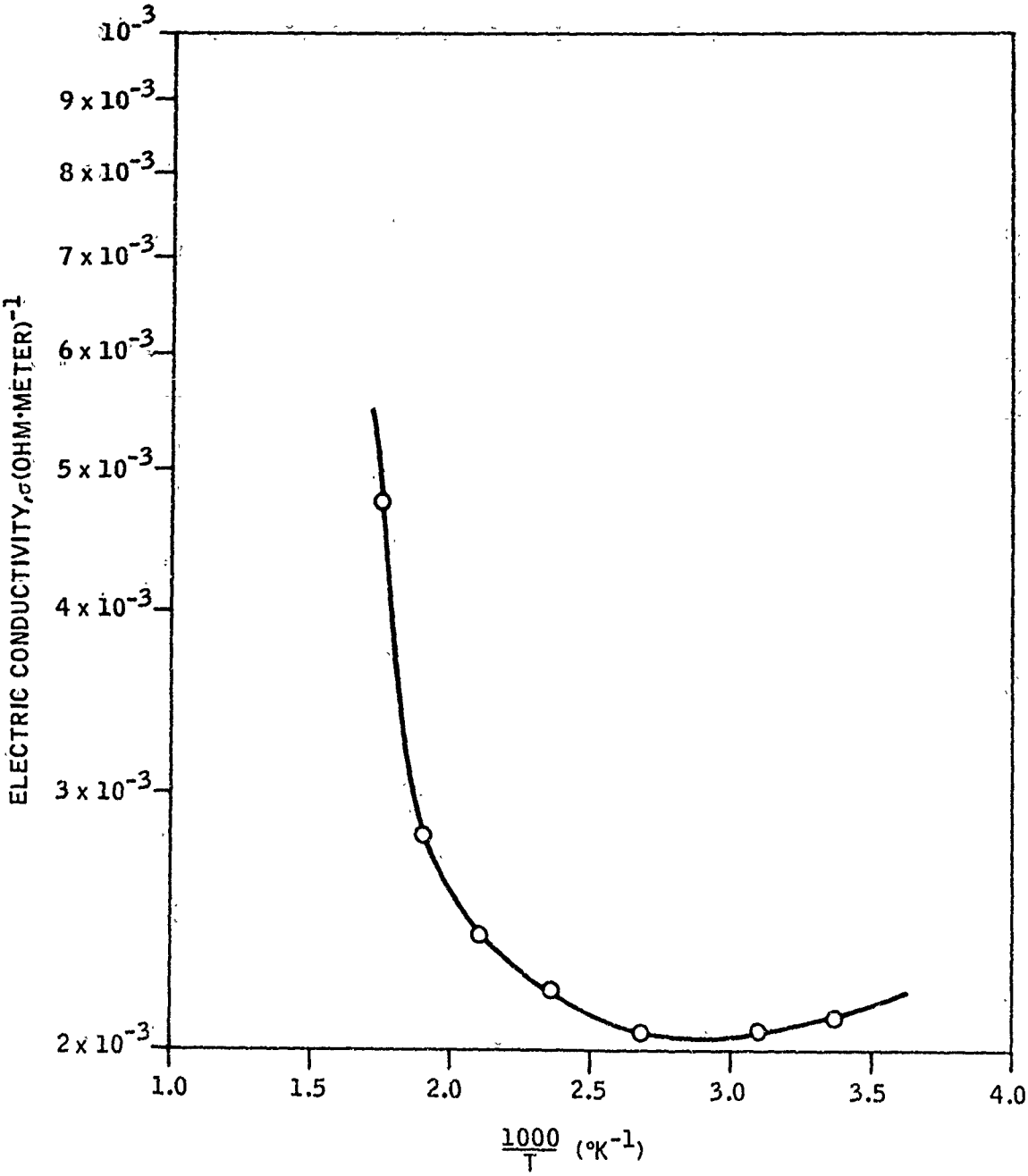

Figure 8-3. Electric Conductivity of Quartzite Showing Anomalous Arrhenius Plot Due to Loss of Water

The electric conductivity, σ, of a specimen containing n mobile particles of charge $\pm ze$ per unit volume is given by

$$\sigma = ze\mu n = \frac{zen\langle\bar{V}\rangle}{n} \tag{8-6}$$

where z is the valence of the conductive particle (or vacancy), and e is the electronic charge.

The diffusion coefficient (D) is related to mobility by the Stokes-Einstein equation (Ref. 7):

$$D = \frac{kT}{ze}\mu \tag{8-7}$$

where k is the Boltzmann constant, and T is the absolute temperature. Combining Equations (8-1), (8-6), and (8-7) leads to

$$\sigma = \omega\varepsilon'' = zen\mu = \frac{(ze)^2 nD}{kT} \tag{8-8}$$

Hence,

$$\varepsilon'' = \frac{(ze)^2 nD}{\omega kT} = \frac{(ze)^2 nD}{2\pi kfT} \tag{8-9}$$

where f is the frequency at which the imaginary component, ε'', of dielectric permittivity, or dielectric loss, is measured.

Diffusion in solid media is regarded as an activated process (Ref. 8) with the diffusion coefficient usually given by

$$D = D_o e^{-Q/RT} \tag{8-10}$$

Equations (8-3), (8-9), and (8-10) show that the activation energy is really the same quantity for dielectric loss, conductance, and diffusion.

Zener and Wert (Ref. 9) made an estimate of the entropic or the pre-exponential term D_o in Equation (8-10) for activated diffusion. They assumed that the diffusion activation energy (Q) is spent in deforming the crystal lattice elastically in the vicinity of the saddle point. Although Zener's treatment applies for metallic lattices, it can be extended to compounds by assuming their lattices to be represented by two interpenetrating elemental lattices. The Zener model also pictures the energy changes associated with diffusional motion as reflected in elastic strains in the lattice. The free energies of formation and motion are accordingly treated as elastic strain energies, and the entropic term is determined from the measured temperature variation of the elastic properties. The frequency factor in Zener's model is accordingly given by

$$D_o = \delta^2 \nu e^{\lambda \xi Q/T_m} \qquad (8\text{-}11)$$

where δ is the average jump distance; ν is the Debye frequency; λ is an empirical constant equal to a 0.55 for substitutional diffusion in fcc lattices, and 1.0 in bcc latticices, and equal to 0.35 for interstitial diffusion; $\xi = -\frac{d \log \mu}{d\left(\frac{T}{T_m}\right)}$ is related to the temperature derivative of the elastic shear modulus μ; Q is the measured activation energy for the diffusion process; and T_m is the melting temperature of the diffusion medium.

The foregoing relationships are given to illustrate that dielectric measurements on rocks can reveal some of their thermophysical and mechanical properties that are obviously needed for scientific optimization of the rock fragmentation process.

SECTION IX

TECHNICAL REPORT SUMMARY AND RECOMMENDATIONS FOR FUTURE WORK

A Boonton 250A RX Bridge was selected to measure the complex permittivity of rock samples over the frequency range 10^7 Hz to 2.5×10^8 Hz. A slotted-line heterodyne detection was assembled for measurement of complex permittivity over the frequency range 10^8 Hz to 4×10^9 Hz. The latter system consists of a GR900LB slotted-line, several GR unit oscillators, an HP sweep oscillator, a crystal mixer, and a 30 MHz IF amplifier-detector.

Accurate dielectric measurements on low-loss rock samples require very precise measurement of high standing-wave ratios with the slotted-line equipment. The square-law detector probe supplied with the slotted line is satisfactory for conventional transmission-line measurements where standing-wave ratios are usually less than 20. However, the detector response did not follow an ideal square-law characteristic at low levels, and the sensitivity was not sufficient for accurate measurements of the minima in the standing-wave pattern. Heterodyne detection was thus used in all of the slotted-line measurements to provide the necessary sensitivity and linearity.

Heterodyne detection requires a separate local-oscillator source in addition to the r-f generator used to drive the transmission line. Both r-f sources must be very stable in frequency to keep the difference frequency centered within the i-f amplifier response curve during the measurement interval. A stable local-oscillator source covering the frequency range above 2 GHz was not available until the end of the contract period, and there was insufficient time to perform the desired measurements in the 2- to 4-GHz range. It should be possible, however, to extrapolate the dielectric constant and loss tangent data considerably beyond the 2-GHz measurement limit because there is no experimental or theoretical evidence of dispersion in this frequency regime.

The 2.45 GHz frequency allocated for industrial, scientific and medical uses is of considerable interest for rock-fragmentation studies. This frequency is well within the valid extrapolation range of the data.

The first coaxial sample holder used in this investigation consisted of GR874 air line with a brass center conductor. Rock samples of basalt, granite, and quartzite in cylindrical form and of the proper outside diameter were provided by the U.S. Bureau of Mines, Twin Cities Mining Research Center. A hole drilled along the cylindrical axis of each rock sample accepts the central conductor of the sample holder. Despite delays due to drilling machine misalignment, drill breakage and nonuniform drill travel, it was possible to secure a few precision drilled samples for use in the slotted line. A second coaxial sample holder consisting of GR900LZ precision air lines and a silver plated center conductor was procured. A new set of rock cylinders to fit the new sample holder was obtained.

Over the frequency range 10^7 to 10^8 Hz, five data points of the complex permittivity were taken for Dresser basalt, charcoal granite, and Sioux quartzite using the RX bridge. The measurements were in error at the higher frequencies due to the invalid lumped-circuit assumptions at these frequencies. Slotted-line measurements were made over the frequency range 3×10^8 to 2×10^9 Hz. Approximately seven data points were collected for each rock type. Measurements were taken at rock sample quarter- and half-wave resonance conditions. Here the rock length limited the low-frequency end of the measurements. Each data point requires a knowledge of the position of the standing wave minimum from the sample input and the width of the wave at that standing wave minimum. The minimum position gives the real part of dielectric permittivity, and the width of the minimum gives a measure of the loss tangent and hence the imaginary part of dielectric permittivity. The least error in measuring the real component of permittivity occurs at half-wave resonance, and the least error in measuring the imaginary component of dielectric permittivity occurs at quarter-wave sample resonance.

Since a lumped circuit approach is invalid above 4×10^7 Hz, transmission-line techniques must be used. Difficulties in measurement then arise due to inaccuracies in line length determinations and nonuniformity of loss parameters throughout the lines. To reduce the uncertainties in dielectric measurements, a method depending on samples of various lengths should be devised in future work to eliminate the need of knowing accurately the length of the transmission line. Slotted-line measurements should be extended outside of the quarter- and half-wave resonance conditions.

The variation of ϵ_r' and ϵ_r'' with frequency for the three rock samples of basalt, granite, and quartzite indicated the absence of dielectric dispersions in the frequency range 10^7 to 10^9 Hz. Hence, dielectric relaxation is absent in rocks at these high frequencies, apparently because the atoms and electrons in the rock are able to faithfully oscillate with the field with no time lag. Dielectric polarization by electron motion results from electrons moving relative to the nucleus in an atom or ion under the influence of an external electric field. The time required for polarization by electron displacement is of the order of 10^{-15} to 10^{-16} second, which requires frequencies much higher than those investigated in this research. Hence, dielectric permittivity of rocks caused by electron displacement shows no dispersion over the whole frequency range from zero to optical frequencies. Polarization by ionic or atomic displacement requires times of the order of 10^{-13} to 10^{-12} second. For a material to exhibit dielectric relaxation due to this type of polarization, frequencies of the order of 10^{12} Hz (0.03 cm wavelength in the infrared part of the spectrum) may be needed. For larger structural units in rocks, dielectric relaxation was found to occur in rocks (last year's research, final report Z9506-3007) in the kHz frequency range. Hence, the displacement of some local structural units (structons) in rocks requires times of the order of 10^{-2} to 10^{-3} second. The absence of dielectric relaxation and the consequent inability to measure rock relaxation times or turnover frequencies in this year's research suggests the absence of smaller structural units in rocks that can resonate in the frequency range 10^7 to 10^9 Hz.

The slotted-line equipment was adapted to enable measurements of rock dielectric parameters at elevated temperatures. The equipment modifications included a temperature-regulated oven, a temperature-isolating section of coaxial line between the slotted-line and sample holder, a heat sink at the input to the slotted line, and an inert gas (argon) supply into the sample holder to prevent corrosion of its inside surfaces.

Rock complex permittivity data were gathered between 25 and 450°C at 50° intervals. Data for basalt could only be taken up to 300°C due to higher order resonance modes that caused inaccurate readings. Data for quartzite could only be taken to 300°C due to rock sample deterioration. No data were taken above 450°C to prevent excessive sample-holder deterioration.

The temperature variation of the real part of dielectric permittivity has been successfully analyzed in the light of the Clausius-Mosotti equation. Dielectric permittivity caused by electronic or atomic displacement is practically independent of temperature. Unless the number density of these elementary particles shows a significant decrease with rise in temperature (as with gases or liquids), the dielectric permittivity of rocks due to electronic or atomic polarization should not change with temperature. The observed change in rock permittivity can therefore be safely assumed to be due to the polarizability of the local structural units (or structons). The change in polarizability (α volume) of these structons with temperature is, therefore, responsible for the change in dielectric permittivity with temperature, their total number remaining constant in a given rock sample. By slightly modifying the terminology of polarizability in the Clausius-Mosotti equation to include the polarizability of the structon (refer to Section VII), it was possible to relate the isobarric thermal expansion coefficient to the temperature coefficient of the relative dielectric constant. On this basis, the volume expansion coefficients of the three rocks investigated have been determined from the temperature coefficient of their relative dielectric constant. The coefficient of volume

expansion of rocks has been found to vary with temperature (Figure 7-1) in an unpredictable manner. In well-behaved systems, thermal expansion coefficients are expected to increase slightly and monotonally with temperature according to the Grüneisen's formula (Ref. 10). Structural and phase transitions in rocks might be responsible for the maxima occuring in their thermal expansion coefficients (Figure 7-1). Validation of these conclusions and of this novel method to determine rock volume expansion coefficients is recommended for future research. Accurate knowledge of the volume expansion coefficient is required for optimization of rock fragmentation processes by a combination of dielectric heating and thermal stress fracturing.

The variation with temperature of the relative dielectric loss was found to follow the Arrhenius relation for basalt and granite. Because dielectric loss is interlinked with electric conductance, the activation energies obtained from the Arrhenius diagrams (Section VIII) would give a measure of the energy height of the "saddle point" for particle diffusion in the rock lattice. Rock mechanical and thermophysical properties can be derived from this type of study in the light of a solid-state diffusion model. For example, the Zener and Wert diffusion model (Ref. 9) can relate the entropic or pre-exponential diffusion term to the Debye frequency and to the temperature derivative of the elastic shear modulus in rocks. The present research illustrates only the beginning steps in this somewhat academic but nevertheless important information on rock thermophysical properties. The relationships between dielectric loss, rock conductivity, diffusivities in rocks, etc., is another area of research that should be pursued by further research.

SECTION X
REFERENCES

1. Von Hipple, Arthur, Dielectric Materials and Applications, Technology Press, Massachusetts Institute of Technology, Cambridge, Mass., 1954.

2. Spalding, H., Ed., "Material-Characteristics Measurement," München 8, West Germany, Rohde Schwartz, Die Kurzinformation 3 + 4/1962.

3. Parkhomenko, E.I., Electrical Properties of Rocks, Plenum Press, New York (1967) pages 20, 24, 25. 144, 148.

4. Huggins, R.A. and Huggins, M.L., "Structural Defect Equilibrium in Vitreous Silica and Dilute Silicates," Journal of Solid-State Chemistry, Vol. 2, 1970, 385-395.

5. Daniel, Vera V., Dielectric Relaxation, Academic Press, London, 1967, p. 212.

6. Menzel, D.H., Fundamental Formulas of Physics, Vol. 2, Dover Publications, Inc., New York, 1960, p. 613.

7. Dekker, A.J., Solid State Physics, Macmillan & Co., Ltd., London, 1958, p. 177.

8. Glasstone, S., J.J. Laidler and H. Eyring, The Theory of Rate Processes, McGraw-Hill, New York, 1951.

9. Zener, C. and C. Wert, "Interstitial Atomic Diffusion Coefficients," Phys. Rev. Vol. 76, 1949, 1169-1175.

10. Gray, E.E., American Institute of Physics Handbook, Second Edition. McGraw-Hill Book Co., Inc., New York (1963), Chapter 4, p. 64.